applied sciences

MDPI

Article

Effects of Diffusion Limitations and Partitioning on Signal Amplification and Sensitivity in Bienzyme Electrochemical Biosensors Employing Cyclic Product Conversion

Romas Baronas * and Karolis Petrauskas

Faculty of Mathematics and Informatics, Institute of Computer Science, Vilnius University, Didlaukio 47, LT-08303 Vilnius, Lithuania; karolis.petrauskas@mif.vu.lt

* Correspondence: romas.baronas@mif.vu.lt

Featured Application

The computational model developed in this study provides a versatile framework for analyzing how enzymatic kinetics, diffusion limitations, and partitioning influence signal amplification and sensitivity in bienzyme electrochemical biosensors employing cyclic product conversion, and it enables optimization of biosensor design parameters for industrial applications.

Abstract

In this study, the nonlinear and non-monotonic behavior of amperometric bienzyme biosensors employing an enzymatic trigger reaction is investigated analytically and computationally using a two-compartment model comprising an enzymatic layer and an outer diffusion layer. The trigger enzymatic reaction is coupled with a cyclic electrochemical–enzymatic conversion (CEC) process. The model is formulated as a system of reaction–diffusion equations incorporating nonlinear Michaelis–Menten kinetics and interlayer partitioning effects. Exact steady-state analytical solutions for substrate and product concentrations, as well as for the output current, are obtained for specific cases of first- and zero-order reaction kinetics. At the transition conditions, biosensor performance is further analyzed numerically using the finite difference method. The CEC biosensor exhibits the highest signal gain when the first enzyme has low activity and the second enzyme has high activity; however, under these conditions, the response time is the longest. When the first enzyme possesses a higher substrate affinity (lower Michaelis constant) than the second, the biosensor demonstrates severalfold higher current and gain compared to the reverse configuration under identical diffusion limitations. Furthermore, increasing external mass transport resistance or interfacial partitioning can enhance the apparent signal gain.

Keywords: amperometric biosensor; signal amplification; trigger reaction; diffusion limitation; transient response; mathematical modeling; computational simulation

Check for updates

Academic Editor: Alexandra Virginia Bounegru

Received: 13 December 2025
Revised: 12 January 2026
Accepted: 21 January 2026
Published: 23 January 2026

Copyright: © 2026 by the authors. Licensee MDPI, Basel, Switzerland. This article is an open access article distributed under the terms and conditions of the Creative Commons Attribution (CC BY) license.

1. Introduction

Biosensors are analytical devices that convert biological interactions into measurable signals [1–3]. In catalytic electrochemical biosensors, an enzyme catalyzes the conversion of the target analyte into an electroactive species, generating an electrical response proportional to the analyte concentration [4–6]. Amperometric enzyme biosensors were the earliest biosensors developed and remain the most widely used due to their simplicity,

ease of fabrication, and low cost. They measure current changes at the working electrode arising from the oxidation or reduction of reaction products, yielding a signal typically proportional to the analyte concentration in solution [2,3,7,8]. In contrast, cyclic voltammetric biosensors monitor the current response as the applied potential is swept cyclically, allowing for comprehensive analysis of redox behavior, electron transfer mechanisms, and the kinetics of enzyme-catalyzed reactions [3,6,9,10]. Owing to their versatility and reliability, enzyme-based electrochemical biosensors have found extensive applications in clinical diagnostics, environmental monitoring, industrial process control, toxin detection, and various other fields [1,5,6,9,11–14].

The detection limit of enzyme electrodes is determined by the sensitivity of amperometric systems [1,2,15,16], which can be substantially improved through the cyclic conversion of substrates or products [2,17–20]. This cyclic conversion is typically achieved using a bienzyme membrane, in which the enzymatic reactions occur in conjunction with the electrochemical process [12,18,21].

If an enzyme initiates analyte conversion through cyclic product conversion, the mechanism of biosensor operation can be described as "triggering" [10,12,22,23]. An example of this type of conversion is the amperometric detection of alkaline phosphatase based on hydroquinone recycling [24]. Another example of utilizing a trigger scheme is the highly sensitive determination of β-galactosidase used as a label in heterogeneous immunoassays [25]. The enzymatic amplification resulting from the triggered, peroxidase-catalyzed conversion of hydrogen peroxide served as the basis for the development of an ultrasensitive hydrogen peroxide biosensor [22]. Zhou et al. developed a sensitive biosensing approach for endopeptidase detection based on analyte-triggered mutual emancipation of linker-immobilized enzymes [23]. This amplification mechanism enabled the detection of extracellular collagenase in bacterial culture supernatants [23].

The mechanism in which an enzymatic substrate conversion (trigger reaction) produces a product that is subsequently electrochemically converted into another product, which is then enzymatically converted back into the first product, is referred to as the CEC mechanism [26,27].

Understanding biosensor kinetics is fundamental to achieving optimal design and performance [28–31]. Mathematical models have been extensively used to analyze the kinetic characteristics of amperometric biosensors that achieve response amplification through cyclic substrate or product conversion [11,18,26,32–35].

Amperometric biosensors utilizing the CEC mechanism have been modeled under both transient [23,27,36,37] and steady-state conditions [26,38]. The analysis is often performed under the assumption of identical substrate affinities for both enzymes (i.e., the same Michaelis constants) [27,36,37,39]. In most cases, the transient models couple enzyme-catalyzed reactions with diffusion processes occurring only within the enzymatic (membrane) layer, while external mass transport by diffusion is neglected [27,36,37].

The external diffusion layer is commonly represented by the Nernst diffusion layer [9,26,40,41]. Single-layer reaction–diffusion models are typically employed under the assumption of a well-stirred bulk solution, such that the Nernst diffusion layer is considered to have zero thickness [42,43]. However, a Nernst diffusion layer of zero thickness cannot be achieved in practice [44]. Nevertheless, single-layer models can be successfully applied to enzyme-based analytical systems with relatively thick enzyme layers, namely when the enzyme layer is at least one order of magnitude thicker than the external diffusion layer [26,43,45]. Otherwise, the external diffusion layer should be explicitly included in the biosensor modeling framework [41,43,45].

Single-layer reaction–diffusion models that neglect external mass transport implicitly assume instantaneous substrate availability at the enzyme layer, which may lead to overes-

timation of reaction rates and sensor responses. Consequently, such models fail to capture diffusion-limited behavior and concentration gradients near the sensor surface, limiting their applicability to realistic experimental conditions [9,41–43].

Diffusion-limiting membranes, such as dialysis, semipermeable, and perforated membranes, are essential for enzyme immobilization and for improving the stability and sensitivity of bioelectrocatalytic systems [2,3]. To achieve sufficient accuracy in describing biosensor systems incorporating diffusion-limiting membranes, multilayer mathematical models that account for partitioning between adjacent layers are required, as external mass transport by diffusion plays a crucial role in determining the dynamics of catalytic processes in enzyme-loaded systems, in general, and biosensor response and sensitivity, in particular [9,14,26,46–51].

In many cases, diffusion through multiple outer layers can be effectively approximated by a single diffusion layer with suitably defined effective diffusion and partition coefficients [52–54]. As a result, two-compartment models are widely used in biosensor modeling [26,42,55–58]. In particular, Coche-Guerente et al. analyzed the amperometric response to phenol of phenol–polyphenol oxidase-based rotating disk bioelectrodes using a two-layer kinetic model that accounts for both internal and external mass transport effects, as well as a CEC electroenzymatic mechanism under steady-state conditions [26].

In two-compartment models, the effects of internal and external diffusion limitations on the response and sensitivity of amperometric biosensors are often investigated under the assumption of perfect contact conditions at the interface between the two layers [42,49,57,59]. However, at a phase boundary, the substrate and product solubilities usually differ between the two materials, leading to discontinuities in the concentration across the interface. In such cases, partition coefficients different from unity must be introduced to account for these effects [26,58,60–63].

The enzymatic amplification arising from the CEC mechanism primarily depends on the activity of the enzyme that reconverts the electrochemically generated product into the initial reactant [26,27,37]. However, the role of enzyme affinity, characterized by the Michaelis constants K_1 and K_2, has not been explicitly addressed; most studies either assume identical constants ($K_1 = K_2$) or examine their effects indirectly, as these parameters are incorporated into dimensionless diffusion quantities such as the Damköhler number or the squared Thiele modulus [27,36–38].

The aim of this work was to investigate the behavior of amperometric bienzyme biosensors utilizing the CEC mechanism in detail, taking into account internal and external diffusion as well as partitioning limitations. Under transient conditions, a biosensor is mathematically modeled using a two-compartment model comprising an enzymatic layer, where the enzymatic reactions and mass transport by diffusion occur, and a diffusion-limiting region, where only mass transport occurs through diffusion. The model is based on a system of reaction–diffusion equations that includes nonlinear terms associated with Michaelis–Menten kinetics of the enzymatic reactions and accounts for partitioning between layers.

Exact analytical solutions for the concentrations of substrate and two reaction products, as well as for the output current, are presented for specific cases of first- and zero-order reaction rates at steady-state. Under the transition conditions, the performance of the biosensor is analyzed numerically using the finite difference method [40,64,65]. The dependence of the apparent Michaelis constant, which reflects biosensor sensitivity and operating range, and of the half-time required to reach steady state, which characterizes the response dynamics, on diffusion limitations, partitioning, and the ratio of the Michaelis constants is investigated here for the first time. The nonlinear effects of partitioning, diffusion lim-

itations, and the ratio of the Michaelis constants on signal amplification and biosensor sensitivity are investigated using both analytical and numerical approaches.

The simulation results are then compared with those obtained for a corresponding mono-enzyme biosensor [27]. Furthermore, the modeled response of the trigger biosensor is compared with that reported in previous studies on biosensors exhibiting the CEC mechanism [26,27,37].

2. Mathematical and Computational Modeling

2.1. Principal Biosensor Structure

Figure 1 presents the treated system schematically, consisting of two relatively thin layers: a bienzyme-loaded membrane applied to the surface of an amperometric electrode followed by an outer diffusion layer [2,9,11].

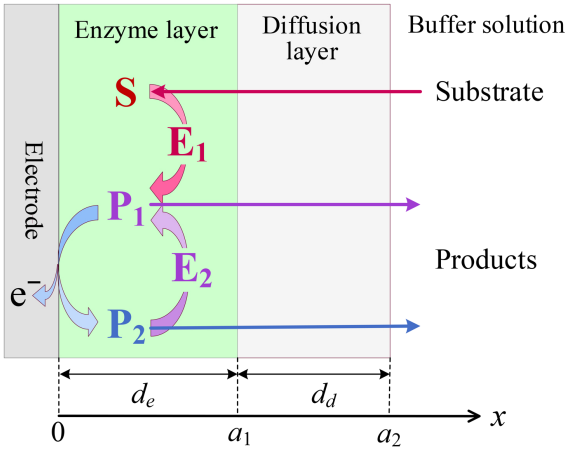


Figure 1. Schematic representation of the investigated system; the figure is not drawn to scale.

In the bienzyme-loaded membrane, two enzyme-catalyzed biochemical reactions occur while electrochemical conversion takes place at the electrode surface [27]:

$$\mathrm{S} \xrightarrow{\mathrm{E_1}} \mathrm{P_1}\,, \tag{1a}$$

$$\mathrm{P_1} \longrightarrow \mathrm{P_2}\,, \tag{1b}$$

$$\mathrm{P_2} \xrightarrow{\mathrm{E_2}} \mathrm{P_1}\,. \tag{1c}$$

In this reaction network, the substrate S is enzymatically converted by enzyme $\mathrm{E_1}$ into product $\mathrm{P_1}$, which is then electrochemically converted into another product $\mathrm{P_2}$. This product $\mathrm{P_2}$ is subsequently enzymatically converted back to $\mathrm{P_1}$ by enzyme $\mathrm{E_2}$.

Under quasi-steady-state approximation (QSSA), the rate R_i of the enzymatic conversion of a substrate S into a product is given by the Michaelis–Menten equation:

$$R_i(S) = \frac{V_i\, S}{K_i + S}\,, \tag{2}$$

where S is the concentration of the substrate S, V_i is the maximal enzymatic rate, and K_i is the Michaelis constant, $i = 1, 2$ [1,2,11,66].

At very low substrate concentrations, where $S \ll K_i$, the nonlinear reaction rate given in (2) simplifies to the first-order reaction rate, $R_i(S) \approx V_i\, S/K_i$. At high substrate concentrations such that $S \gg K_i$, the rate becomes independent of the substrate concentration, exhibiting zero-order kinetics, $R_i(S) \approx V_i$, $i = 1, 2$.

Biochemical reactions in practical biosensors are influenced by factors such as pH, enzyme loading, cofactor availability, temperature, and enzyme degradation [1–3,7]. Under defined conditions, these effects are commonly incorporated into the Michaelis–Menten parameters and introduced empirically, even though they lie outside the original formulation. In biosensor modeling, the resulting modified parameters are typically referred to as "apparent" or "effective" [9,11,43].

In the two-layer (two-compartment) models, the diffusion layer is most commonly represented by the Nernst diffusion layer [9,26,40,41]. When the external Nernst layer is neglected, mass transport can alternatively be described by a semi-permeable, diffusion-limiting membrane [33,40,42,43,49,67]. It should be noted, however, that a Nernst diffusion layer of zero thickness is not physically realizable [44].

In some biosensor models, both the outer membrane and the Nernst diffusion layer are explicitly included [42,53,54,60,68]. Nevertheless, mass transport across multiple diffusion layers can often be effectively approximated by a single equivalent layer with apparent diffusion and partition coefficients, enabling reduction of a multi-compartment system to an effective two-compartment model [52–54]. Accordingly, the results presented in this study are also applicable to amperometric biosensors incorporating multiple diffusion layers, including systems that explicitly account for both the outer membrane and the Nernst diffusion layer.

2.2. Mathematical Model

Assuming symmetric geometry of the electrode, enzyme, and diffusion layers, together with a uniform distribution of the immobilized enzyme within the enzyme membrane, a two-layer model can be formulated in a one-dimensional spatial domain. The model is posed as an initial–boundary value problem describing the dynamics of substrate and product concentrations [11,42,43,69].

2.2.1. Governing Equations

The temporal variations in the concentrations of the substrate S and products P_1 and P_2 within the enzyme layer are governed by a system of reaction–diffusion equations for $t > 0$,

$$\frac{\partial S_e}{\partial t} = D_{S_e}\frac{\partial^2 S_e}{\partial x^2} - R_1(S_e)\,, \tag{3a}$$

$$\frac{\partial P_{1e}}{\partial t} = D_{P_{1e}}\frac{\partial^2 P_{1e}}{\partial x^2} + R_1(S_e) + R_2(P_{2e})\,, \tag{3b}$$

$$\frac{\partial P_{2e}}{\partial t} = D_{P_{2e}}\frac{\partial^2 P_{2e}}{\partial x^2} - R_2(P_{2e}), \quad x \in (0,\, a_1), \tag{3c}$$

where x and t stand for space and time, respectively; $S_e(x,t)$ and $P_{ie}(x,t)$ are the molar concentrations of the substrate and product in the enzyme layer, respectively; D_{S_e} and $D_{P_{ie}}$ are the diffusion coefficients; and $a_1 = d_e$ is the thickness of the enzyme layer, $i = 1, 2$ [11,26,27,42].

In the second (diffusion) layer, only mass transport by diffusion occurs ($t > 0$),

$$\frac{\partial S_d}{\partial t} = D_{S_d}\frac{\partial^2 S_d}{\partial x^2}\,, \tag{4a}$$

$$\frac{\partial P_{1d}}{\partial t} = D_{P_{1d}}\frac{\partial^2 P_{1d}}{\partial x^2}\,, \tag{4b}$$

$$\frac{\partial P_{2d}}{\partial t} = D_{P_{2d}}\frac{\partial^2 P_{2d}}{\partial x^2}\,, \quad x \in (a_1,\, a_2), \tag{4c}$$

where $S_d(x,t)$ and $P_{id}(x,t)$ are the concentrations of the substrate and the reaction products in the diffusion layer, D_{S_d} and $D_{P_{id}}$ are the diffusion coefficients, $a_2 = a_1 + d_d$, and d_d is the thickness of the diffusion layer [11,42,43].

2.2.2. Initial and Boundary Conditions

The operation of the biosensor begins when the analyte (substrate) is introduced into the buffer solution at $t = 0$:

$$S_e(x,0) = 0,\ x \in [0, a_1]; \quad S_d(x,0) = 0,\ x \in [a_1, a_2); \quad S_d(a_2, 0) = S_0, \tag{5a}$$

$$P_{1e}(x,0) = 0,\ x \in [0, a_1]; \quad P_{1d}(x,0) = 0,\ x \in [a_1, a_2], \tag{5b}$$

$$P_{2e}(x,0) = 0,\ x \in [0, a_1]; \quad P_{2d}(x,0) = 0,\ x \in [a_1, a_2], \tag{5c}$$

where S_0 is the concentration of the substrate in the bulk solution [26,27].

The substrate is assumed to be electro-inactive. The electrode potential is chosen to maintain a product concentration P_1 of zero at the electrode surface. Because of the electrochemical reaction, the rate of generation for the second product P_2 at the electrode surface is equal to the conversion rate of product P_1. These relationships are used in the boundary conditions ($t > 0$) defined at the electrode surface ($x = 0$) [26,27],

$$D_{S_e} \frac{\partial S_e}{\partial x}\Big|_{x=0} = 0\,, \tag{6a}$$

$$P_{1e}(0,t) = 0\,, \tag{6b}$$

$$D_{P_{2e}} \frac{\partial P_{2e}}{\partial x}\Big|_{x=0} = -D_{P_{1e}} \frac{\partial P_{1e}}{\partial x}\Big|_{x=0}\,. \tag{6c}$$

During biosensor operation, the concentrations of the substrate and products in the bulk solution are assumed to be time-independent for $t > 0$ [26,27],

$$S_d(a_2,t) = S_0\,, \tag{7a}$$

$$P_{1d}(a_2,t) = 0\,, \tag{7b}$$

$$P_{2d}(a_2,t) = 0\,. \tag{7c}$$

At the interface between adjacent layers, the fluxes of the substrate and products are assumed to be continuous; that is, the outgoing flux from one layer equals the incoming flux to the next. However, the concentrations on either side of each interface may differ and are related through the formal partition coefficients:

θ_S for the substrate and θ_{P_1} and θ_{P_2} for the products ($t > 0$) [26,58,60,61,63,69],

$$D_{S_e} \frac{\partial S_e}{\partial x}\Big|_{x=a_1} = D_{S_d} \frac{\partial S_d}{\partial x}\Big|_{x=a_1}, \tag{8a}$$

$$S_e(a_1,t) = \theta_S S_d(a_1,t), \tag{8b}$$

$$D_{P_{1e}} \frac{\partial P_{1e}}{\partial x}\Big|_{x=a_1} = D_{P_{1d}} \frac{\partial P_{1d}}{\partial x}\Big|_{x=a_1}, \tag{8c}$$

$$P_{1e}(a_1,t) = \theta_{P_1} P_{1d}(a_1,t), \tag{8d}$$

$$D_{P_{2e}} \frac{\partial P_{2e}}{\partial x}\Big|_{x=a_1} = D_{P_{2d}} \frac{\partial P_{2d}}{\partial x}\Big|_{x=a_1}, \tag{8e}$$

$$P_{2e}(a_1,t) = \theta_{P_2} P_{2d}(a_1,t). \tag{8f}$$

In the limit $a_2 \to a_1$ ($d_d \to 0$), the two-compartment model defined by Equations (3)–(8) reduces to the corresponding single-compartment model [27,35,37].

2.3. Biosensor Characteristics

The amperometric electrode senses the faradaic current, which may be anodic or cathodic. An explicit expression for the current density I follows from Faraday's and Fick's laws and is determined by the flux of the reaction product at the electrode surface,

$$I(t) = n_e F D_{P_{1_e}} \frac{\partial P_{1e}}{\partial x}\bigg|_{x=0} = -n_e F D_{P_{2_e}} \frac{\partial P_{2e}}{\partial x}\bigg|_{x=0}, \tag{9}$$

where n_e denotes the number of electrons transferred at the electrode surface and F is the Faraday constant, with $F = 96485$ C/mol [11,18,26,42].

As $t \to \infty$, the system (3)–(8) approaches a steady-state solution [11,27,42,66],

$$S_{e\mathrm{ss}}(x) = \lim_{t\to\infty} S_e(x,t), \quad S_{d\mathrm{ss}}(x) = \lim_{t\to\infty} S_d(x,t), \tag{10a}$$

$$P_{1e\mathrm{ss}}(x) = \lim_{t\to\infty} P_{1e}(x,t), \quad P_{1d\mathrm{ss}}(x) = \lim_{t\to\infty} P_{1d}(x,t), \tag{10b}$$

$$P_{2e\mathrm{ss}}(x) = \lim_{t\to\infty} P_{2e}(x,t), \quad P_{2d\mathrm{ss}}(x) = \lim_{t\to\infty} P_{2d}(x,t), \tag{10c}$$

$$I_{\mathrm{ss}} = \lim_{t\to\infty} I(t), \tag{10d}$$

where $S_{e\mathrm{ss}}$, $S_{d\mathrm{ss}}$, $P_{ie\mathrm{ss}}$, and $P_{id\mathrm{ss}}$ are the steady-state concentrations of the substrate and products, where $i = 1, 2$, and I_{ss} is the density of the steady-state output current.

The half-time $T_{0.5}$, defined as the time required for the current to reach half of its steady-state value, is commonly used to assess the dynamic performance of biosensors [43],

$$T_{0.5} = \{t : I(t) = 0.5 I_{\mathrm{ss}}\}. \tag{11}$$

The half-time $T_{0.5}$ serves as a kinetic measure of the biosensor response rate, reflecting the combined effects of diffusion and reaction processes that determine how rapidly the steady-state current is established.

The sensitivity is a key characteristic of the biosensor response [1,2,70]. It is commonly defined as the slope of the steady-state output current with respect to the measured substrate concentration S_0 [70]. Accordingly, the sensitivity $B_{\mathrm{s}}(S_0)$ and the corresponding dimensionless sensitivity $B_{\mathrm{s}}^*(S_0)$ with respect to S_0 are defined as [43]

$$B_{\mathrm{s}}(S_0) = \frac{\partial I_{\mathrm{ss}}(S_0)}{\partial S_0}, \quad B_{\mathrm{s}}^*(S_0) = B_{\mathrm{s}}(S_0) \times \frac{S_0}{I_{\mathrm{ss}}(S_0)}, \tag{12}$$

where $I_{\mathrm{ss}}(S_0)$ is the density of the steady-state current calculated at the substrate concentration S_0.

The apparent Michaelis constant K_{app} is commonly regarded as a characteristic parameter describing both the sensitivity and the calibration curve of amperometric biosensors [2,39,50,66,70]. A higher value of K_{app} indicates a broader linear range of the calibration curve. By definition, K_{app} represents the substrate concentration at which the biosensor response reaches half of its maximum value, under the assumption that the substrate concentration tends to infinity while all other model parameters remain fixed [43],

$$K_{\mathrm{app}} = \left\{ \bar{S}_0 : I_{\mathrm{ss}}(\bar{S}_0) = 0.5 \lim_{S_0\to\infty} I_{\mathrm{ss}}(S_0) \right\}. \tag{13}$$

In the special case in which $V_2 = 0$, i.e., when $R_2(P_{2_e}) \equiv 0$, reaction (1c) is absent. Consequently, the reaction network (1) reduces to the two reactions (1a) and (1b), which fol-

low a CE scheme and occur in a conventional mono-enzyme biosensor [2,3,7,8,22,32]. The mathematical model (3)–(8) can then be simplified to a two-layer amperometric biosensor model with four governing equations—(3a), (3b), (4a), and (4b)—together with the boundary conditions (6a), (6b), (7a), (7b), and (8a)–(8d), and the initial conditions (5a) and (5b). The output current density is then calculated from the concentration of P_{1e}, as defined in (9). The effects of partitioning and diffusion limitations on the response of such conventional amperometric biosensors have already been investigated in detail using a two-layer and, more generally, three-layer models [42,49,54].

To investigate the effect of signal amplification, one of the key characteristics of the trigger biosensors, the response of the trigger biosensor employing the CEC scheme, was compared with that of the corresponding conventional biosensor based on the CE scheme. The dimensionless ratio (also called the signal gain) of the steady-state current of the trigger biosensor to that of the corresponding CE biosensor was used as a quantitative measure of amplification,

$$G(S_0, V_1, V_2) = \frac{I_{ss}(S_0, V_1, V_2)}{I_{ss}(S_0, V_1, 0)}, \tag{14}$$

where $I_{ss}(S_0, V_1, V_2)$ is the steady-state current density of the trigger biosensor, obtained for the substrate concentration S_0 at the maximal activity V_i of an enzyme E_i, $i = 1, 2$ [27].

2.4. Dimensionless Model Parameters

To determine the principal parameters of the mathematical model, a dimensionless formulation is typically derived [40,41,60]. In this study, the two-compartment model (3)–(8) was nondimensionalized by rescaling time, space, diffusion coefficients, and concentrations [26,43,49,54]. This transformation yielded the following dimensionless governing parameters:

$$\begin{aligned}
&x^* = \frac{x}{d_e}, \quad t^* = \frac{D_{\text{ref}}\, t}{d_e^2}, \quad \kappa = \frac{K_2}{K_1}, \\
&S_e^* = \frac{S_e}{K_1}, \quad S_d^* = \frac{S_d}{K_1}, \quad \sigma_1^2 = \frac{V_1 d_e^2}{K_1 D_{S_e}}, \quad \beta_S = \frac{D_{S_d} d_e}{\theta_S D_{S_e} d_d}, \\
&P_{ie}^* = \frac{P_{ie}}{K_i}, \quad P_{id}^* = \frac{P_{id}}{K_i}, \quad \sigma_2^2 = \frac{V_2 d_e^2}{K_2 D_{P_{2e}}}, \quad \beta_{P_i} = \frac{D_{P_{id}} d_e}{\theta_{P_i} D_{P_{ie}} d_d}, \quad i = 1, 2, \\
&I^*(t^*) = \frac{D_{P_{1e}}}{D_{\text{ref}}} \frac{\partial P_{1e}^*}{\partial x^*}\bigg|_{x^*=0} = \frac{I(t)\, d_e}{n_e F D_{\text{ref}} K_1}, \quad I_{ss}^* = \lim_{t^* \to \infty} I^*(t^*),
\end{aligned} \tag{15}$$

where D_{ref} is the reference diffusion coefficient representing the characteristic diffusivity of the system; κ denotes the ratio of Michaelis constants; σ_i^2 is the dimensionless Damköhler number (i.e., the square of the Thiele modulus, also known as the diffusion module); and β_S and β_{P_i} represent the Biot numbers for the substrate and products, respectively ($i = 1, 2$) [18,42,71,72]. The nondimensionalized form of the model Equations (3)–(8) is presented in Appendix A, and the corresponding dimensional and dimensionless parameters are summarized in Table A1.

The ratio $\kappa = K_2/K_1$ compares the effective substrate affinities of the two enzymes within the coupled enzymatic–electrochemical system (1). A smaller value of κ indicates that the enzyme E_2 binds its substrate P_2 more tightly than enzyme E_1 binds S, whereas a larger κ implies weaker binding. Thus, the ratio provides insight into how reaction rates are balanced between the two enzymatic steps [4,8].

The dimensionless parameter σ_i^2 quantifies the balance between enzymatic activity and substrate (or product) transport. It represents the ratio of the intrinsic enzymatic reaction rate (V_i/K_i) to the rate of substrate (D_{S_e}/d_e^2) or product ($D_{P_{2e}}/d_e^2$) diffusion through the enzyme layer, where $i = 1, 2$. For a bienzyme biosensor, when each $\sigma_i^2 \ll 1$ ($i = 1, 2$), the

biosensor response is dominated by enzyme kinetics. Conversely, for $\sigma_i^2 \gg 1$, the response is primarily controlled by the limitations of internal diffusion [3,11,42,48,72].

The Biot numbers β_S, β_{P_1}, and β_{P_2} are dimensionless parameters that quantify the balance between internal and external mass transport resistances [9,46,48,71]. Because substrates and products often exhibit different diffusion properties, distinct Biot numbers are sometimes defined for each species. For simplicity, however, they are frequently assumed to be identical [46,49,54]. A large Biot number indicates that diffusion within the enzyme layer is slower than in the external diffusion layer, while a small Biot number implies that mass transport in the surrounding layer is more restrictive [9,48,71].

3. Solving the Model

Because of the nonlinear nature of the governing Equation (3), the initial–boundary value problem (3)–(8) admits analytical solutions only for specific parameter sets [40,42]. Consequently, the problem was solved numerically in the general case. For the particularly important cases of first- and zero-order reaction rates under steady-state conditions, Equations (3)–(8) were also solved analytically. These exact solutions were then used to validate the numerical solution obtained for the general case.

3.1. Relationship Between Steady-State Concentrations

At the steady-state ($t \to \infty$), the governing Equation (3) yield a relationship between the species concentrations in the enzyme layer [26,27],

$$D_{S_e}\frac{\partial^2 S_e}{\partial x^2} + D_{P_{1e}}\frac{\partial^2 P_{1e}}{\partial x^2} + D_{P_{2e}}\frac{\partial^2 P_{2e}}{\partial x^2} = 0, \quad x \in (0, a_1). \tag{16}$$

Integrating this equation and applying boundary conditions (6) result in the following relationship between steady-state concentrations in the enzyme layer:

$$D_{S_e}S_{e\mathrm{ss}} + D_{P_{1e}}P_{1e\mathrm{ss}} + D_{P_{2e}}P_{2e\mathrm{ss}} = D_{S_e}S_{e\mathrm{ss}}(0) + D_{P_{2e}}P_{2e\mathrm{ss}}(0), \quad x \in [0, a_1]. \tag{17}$$

Similarly, combining (4) with the boundary conditions (7) yields the following relationship among the steady-state concentrations in the diffusion layer:

$$D_{S_d}S_{d\mathrm{ss}} + D_{P_{1d}}P_{1d\mathrm{ss}} + D_{P_{2d}}P_{2d\mathrm{ss}} = D_{S_d}S_0, \quad x \in [a_1, a_2]. \tag{18}$$

As a special case, this constraint holds at the interface between two layers. By applying (8b), (8d), and (8f), it can be expressed in terms of enzyme layer concentrations,

$$D_{S_d}S_{e\mathrm{ss}}/\theta_S + D_{P_{1d}}P_{1e\mathrm{ss}}/\theta_{P_1} + D_{P_{2d}}P_{2e\mathrm{ss}}/\theta_{P_2} = D_{S_d}S_0, \quad x = a_1. \tag{19}$$

3.2. Steady-State Analytical Solution

One can see that the boundary value problem (3)–(8) for the substrate concentration can be solved separately from the other concentrations. The initial–boundary value problem in (3a), (4a), (5a), (6a), (7a), (8a), and (8b) is typical for two-compartment models of amperometric and potentiometric biosensors [26,60]. The stationary ($t \to \infty$) analytical solution had already been derived for a more general three-layer mathematical model involving partitioning [54,73].

Having the steady-state solution to the problem (3)–(8) for the substrate, a solution for the second product P_2 can be derived very similarly, as the governing equations are of the same form. Just the boundary condition at the electrode surface is of a different type.

To streamline the analysis, we adopt species-independent diffusion and partition coefficients for a standard simplification [26,32,35,37,38,54,60],

$$\begin{gathered} D_e = D_{\text{ref}} = D_{S_e} = D_{P_{1e}} = D_{P_{2e}}, \quad D_d = D_{S_d} = D_{P_{1d}} = D_{P_{2d}}, \\ \theta = \theta_S = \theta_{P_1} = \theta_{P_2}, \quad \beta = \beta_S = \beta_{P_1} = \beta_{P_2}. \end{gathered} \tag{20}$$

In real biosensing systems, different species may exhibit distinct diffusion coefficients and partitioning behaviors [47,61,62]. However, the substrate and enzymatic products are typically small, low-molecular-weight species with comparable molecular sizes, shapes, and charges (e.g., hydroquinone, phenol, and catechol), resulting in similar diffusion coefficients [24,26,32]. Because partitioning at a membrane–solution interface is governed primarily by molecular size, hydrophobicity, and charge, species with similar physicochemical properties are expected to exhibit similar partition coefficients. Importantly, the qualitative trends and mechanistic insights derived from the model are primarily governed by the relative timescales of reaction and transport, rather than by precise, species-specific parameter values. Moreover, experimental measurements of diffusion and partition coefficients for individual species in enzyme layers are limited [39,47,61,62,67].

Assuming equal diffusion and partition coefficients is a physically reasonable approximation that simplifies the model without significantly compromising accuracy, particularly when the objective is to capture general trends, scaling behavior, or limiting regimes rather than species-specific transport effects. For example, Coche-Guerente et al. applied species-independent diffusion and partition coefficients in their analysis of the catechol–polyphenol oxidase and phenol–polyphenol oxidase systems [26,32], while Velkovsky et al. adopted the same assumption for enzyme electrodes based on glucose oxidase and lactate oxidase [60]. This assumption is also typical in the theoretical analysis of biosensors employing a trigger scheme [9,27,35–38]. Overall, adopting species-independent diffusion and partition coefficients reduces the number of free parameters and helps avoid overfitting, while maintaining adequate model fidelity.

Under assumption (20), by combining constraint (19) with (17) at $x = a_1$, a relationship involving the substrate and the second product at the electrode surface ($x = 0$) can be derived and expressed as the boundary condition for P_2 at $x = 0$, which is used to solve the stationary problem for the second product,

$$P_{2e\text{ss}}(0) = \theta S_0 - S_{e\text{ss}}(0). \tag{21}$$

Having obtained the solutions for the substrate and product P_2, the concentration of product P_1 can be determined using (17) and (18),

$$P_{1e\text{ss}}(x) = \theta S_0 - S_{e\text{ss}}(x) - P_{2e\text{ss}}(x), \quad x \in [0, a_1], \tag{22a}$$

$$P_{1d\text{ss}}(x) = S_0 - S_{d\text{ss}}(x) - P_{2d\text{ss}}(x), \quad x \in [a_1, a_2]. \tag{22b}$$

3.2.1. Solution for First-Order Reaction Rates

Applying the known analytical solution of the three-layer mathematical model yields the following expressions for the substrate concentrations corresponding to first-order reaction rates in the two layers [54,73]:

$$S_{e\text{ss}}(x) = \theta S_0 \cosh(\alpha_1 x)/\mathcal{A}, \tag{23a}$$

$$S_{d\text{ss}}(x) = S_0 \left(\cosh(\sigma_1) + \frac{x - a_1}{d_d} \sigma_1 \sinh(\sigma_1)/\beta \right) / \mathcal{A}, \tag{23b}$$

where

$$\mathcal{A} = \cosh(\sigma_1) + \sigma_1 \sinh(\sigma_1)/\beta\,, \quad \alpha_1 = \sigma_1/d_e\,. \tag{24}$$

Solving the boundary value problem (3c), (4c), (7c), (8e), (8f) and (21) leads to the following expressions of the concentration of the reaction product P_2:

$$P_{2e\mathrm{ss}}(x) = \theta S_0(1 - 1/\mathcal{A})(\cosh(\alpha_2 x) - \mathcal{B}\sinh(\alpha_2 x)), \tag{25a}$$

$$P_{2d\mathrm{ss}}(x) = S_0(1 - 1/\mathcal{A})\big(\cosh(\sigma_2) - \mathcal{B}\sinh(\sigma_2)\big)\frac{a_2 - x}{d_d}, \tag{25b}$$

where

$$\mathcal{B} = \frac{\cosh(\sigma_2) + \sigma_2 \sinh(\sigma_2)/\beta}{\sinh(\sigma_2) + \sigma_2 \cosh(\sigma_2)/\beta}, \quad \alpha_2 = \sigma_2/d_e\,. \tag{26}$$

Having the concentration of the second product as defined in (25a), the steady-state current I_{ss} can be found from (9),

$$I_{\mathrm{ss}} = n_e F D_e \theta S_0 \alpha_2 \left(1 - \frac{1}{\mathcal{A}}\right)\mathcal{B} = n_e F \theta S_0 \frac{D_e}{d_e}\left(1 - \frac{1}{\mathcal{A}}\right)\sigma_2 \mathcal{B}\,. \tag{27}$$

In the special case $\alpha_2 = 0$ ($\sigma_2 = 0$, $R_2 = 0$, $P_{2e} \equiv 0$), the steady-state concentrations $P_{1e\mathrm{ss}}$ and $P_{1d\mathrm{ss}}$ of product P_1, as defined in (22) and (25), and the steady-state output current I_{ss}, as defined in (27), can be reduced to the known expressions for the corresponding two-layer CE biosensor [54] because

$$\begin{aligned} &\lim_{\alpha_2 \to 0} \alpha_2 \mathcal{B} = \frac{\beta}{\beta + 1}\frac{1}{d_e}, \quad \lim_{\alpha_2 \to 0} \sinh(\alpha_2 x)\mathcal{B} = \frac{\beta}{\beta + 1}\frac{x}{d_e}, \\ &\lim_{\alpha_2 \to 0} \sigma_2 \mathcal{B} = \lim_{\sigma_2 \to 0} \sigma_2 \mathcal{B} = \frac{\beta}{\beta + 1}\,. \end{aligned} \tag{28}$$

The derived expressions (23a) and (25a) for the concentrations within the enzyme layer agree well with those reported by Coche-Guerente et al. [26]. Additionally, assuming $d_d \to 0$ ($\beta \to \infty$), $\theta = 0$, and $\sigma_1^2 \gg 1$, the derived solution (23)–(27) converges to that of the corresponding one-compartment model [37].

3.2.2. Solution for Zero-Order Reaction Rates

By applying the known analytical solution of the three-layer mathematical model [54,73], the following expressions for the substrate concentrations under zero-order reaction kinetics in the two layers are obtained:

$$S_{e\mathrm{ss}}(x) = \theta S_0 - (0.5(d_e^2 - x^2)/d_e^2 + 1/\beta)\sigma_1^2 K_1, \tag{29a}$$

$$S_{d\mathrm{ss}}(x) = S_0 - (a_2 - x)/(d_d \theta \beta)\sigma_1^2 K_1. \tag{29b}$$

Solving the boundary value problem (3c), (4c), (7c), (8e), (8f), and (21) for zero-order reaction rates yields the following expressions for the concentration of reaction product P_2:

$$P_{2e\mathrm{ss}}(x) = 0.5\sigma_2^2 K_2 \frac{x^2}{d_e^2} - \Big(\sigma_2^2 K_2(0.5\beta + 1) + P_{2e\mathrm{ss}}(0)\beta\Big)\frac{x}{d_e(1 + \beta)} + P_{2e\mathrm{ss}}(0), \tag{30a}$$

$$P_{2d\mathrm{ss}}(x) = \Big(P_{2e\mathrm{ss}}(0) - 0.5\sigma_2^2 K_2\Big)\frac{a_2 - x}{\theta d_d(1 + \beta)}, \tag{30b}$$

where

$$P_{2e\mathrm{ss}}(0) = \sigma_1^2 K_1 \frac{0.5\beta + 1}{\beta}. \tag{31}$$

The steady-state current is then expressed as follows:

$$I_{ss} = n_e F \frac{D_e(2+\beta)}{2d_e(1+\beta)}\left(\sigma_2^2 K_2 + \sigma_1^2 K_1\right) = n_e F \frac{d_e(V_1+V_2)}{2}\frac{(2+\beta)}{(1+\beta)}. \quad (32)$$

Similarly to the case of first-order reaction rates, the solution (29)–(32) generalizes the known expressions for the corresponding two-layer CE biosensor [54] and for the one-compartment CEC biosensor model with zero-order reaction rates [37].

The derived expression (32) shows that the steady-state current is invariant with respect to the substrate concentration S_0 when $S_0 \gg K_1$ and $S_0 \gg K_2$. This well-known feature of enzyme-based biosensors indicates their insensitivity for extremely high analyte concentrations, i.e., $B_s^*(S_0) = 0$. However, when semi-analytical techniques are applied to solve nonlinear mathematical models, such as in the case of the CEC biosensor, an approximate analytical expression for the output current can include S_0 even for zero-order reaction rates [37].

3.3. Transient Numerical Simulation

To obtain a numerical solution of the nonlinear model (3)–(8), a non-uniform spatial–temporal grid was employed. A semi-implicit linear finite-difference scheme was formulated based on discrete approximations of the governing equations [27,43,65]. The diffusion terms were treated implicitly, whereas the reaction terms were handled explicitly. The resulting tridiagonal systems of linear algebraic equations were solved efficiently using the Thomas algorithm [40]. At each discrete time level, the algebraic systems were first solved for the substrate and the first product, after which the system for the second product was solved using the computed surface concentration of the first product, as required by the boundary condition (6c).

The resulting finite-difference scheme is unconditionally stable with respect to diffusion. However, the explicit treatment of the nonlinear Michaelis–Menten reaction terms imposes a time-step restriction. In particular, to ensure stability and nonnegativity of the numerical solution, the time step Δt was chosen to satisfy $\Delta t \leq \min(K_1/V_1, K_2/V_2)$ in accordance with standard stability criteria for explicit reaction discretizations [40,64,65]. To ensure numerical accuracy, refined spatial discretization was applied in the vicinity of the boundaries $x = 0$, $x = a_1$, and $x = a_2$, where concentration gradients are steep [43,54]. The intervals $[0, a_1]$ and $[a_1, a_2]$ were discretized using a spatial step situation with more than $10,000$ individual responses, discussed below.

Although the time step was constrained by the partition (matching) conditions (8) [63], it was reasonable to employ a progressively increasing step size in the time direction [74], since the biosensor operation ultimately satisfies the steady-state assumption as $t \to \infty$. The final time step was several orders of magnitude larger than the initial one [49,54,73]. The steady-state current density I_{ss} was approximated by the instantaneous current value at time T_{ss}, defined as the earliest time at which the normalized absolute current slope falls below a prescribed small threshold of $\varepsilon = 10^{-3}$ [42,43]. Specifically,

$$T_{ss} = \min_{I(t)>0}\left\{t : \frac{t}{I(t)}\left|\frac{\partial I(t)}{\partial t}\right| < \varepsilon\right\}, \quad I_{ss} \approx I(T_{ss}). \quad (33)$$

The numerical simulator was programmed in Java language [75]. The simulation results were then visualized using Origin 2025b [76].

The numerical solution was validated by comparison with exact analytical solutions obtained for specific cases of first- and zero-order reaction kinetics under steady-state conditions, as presented in Section 3.2. The relative error of the steady-state current

remained below 0.5% over a wide range of model parameter values. The error increased with stronger internal diffusion limitations, corresponding to higher values of σ_1^2 and σ_2^2. At $\sigma_1^2 = \sigma_2^2 = 100$, the relative error reached 1.5%. Doubling the minimum spatial step size increased the relative error to 3.3%, whereas halving the size reduced the error to 0.8%.

Additional validation was performed by benchmarking against numerical solutions for a two-layer amperometric biosensor model in the limiting case $V_2 = 0$ [42,49]. Furthermore, approximate analytical solutions and numerical results reported for the corresponding one-compartment biosensor model operating in trigger mode under transient conditions were used to further verify the accuracy of the proposed numerical approach [27,35,37].

4. Results and Discussion

To investigate the behavior of amperometric enzyme-based biosensors employing the CEC mechanism and accounting for both internal and external diffusion limitations, the biosensor response was simulated over a wide range of key dimensionless model parameters, assuming species-independent diffusion and partition coefficients as defined in (20) and using the following typical dimensional parameter values [4,22,27,49,51,54],

$$\begin{gathered} D_e = 400\,\mu\text{m}^2/\text{s}, \quad D_d = 600\,\mu\text{m}^2/\text{s}, \\ d_e = 20\,\mu\text{m}, \quad S_0 = K_1 = 100\,\mu\text{M}, \quad n_e = 1. \end{gathered} \tag{34}$$

we approximated the ranges of the dimensionless parameters employed in this work, estimated from representative literature data for dual-enzyme amperometric biosensors, summarized in Table A2. Parameter intervals were additionally explored to analyze limiting transport and kinetic regimes and to evaluate the generality of the model predictions.

The biosensor response was numerically simulated at the mean substrate concentration ($S_0 = K_1$). For low ($S_0 \ll K_1$) and high ($S_0 \gg K_1$) substrate concentrations, the response is accurately described by the exact analytical solutions given in Section 3.2.

4.1. Temporal Dynamics of the Biosensor Response

Figure 2 shows the steady-state and half-time ($T_{0.5}$) concentration profiles of the substrate and both products, as well as the evolution of the biosensor current I. The biosensor response was numerically simulated for three maximal enzymatic rates V_1 and V_2, namely 10, 100, and 1000 μM/s (with $V_1 = V_2$). The simulations assumed identical Michaelis constants ($K_2 = K_1$, $\kappa = 1$), an external diffusion layer thickness of $d_d = 2d_e = 40$ μm, and a partition coefficient of $\theta = 0.75$. All other model parameters were as defined in (34). Under these conditions, variations in maximal enzymatic rates cause the biosensor operation to shift from enzyme kinetics limitation to internal diffusion limitation, as both diffusion modules σ_1^2 and σ_2^2 increase from 0.1 to 10. At intermediate values of $V_1 = V_2 = 100\,\mu\text{M/s}$, the biosensor operates under mixed control involving internal diffusion and the kinetics of the two enzymes, E_1 and E_2 ($\sigma_1^2 = \sigma_2^2 = 1$). Furthermore, mass transport in the outer diffusion layer is comparable to that in the enzyme layer, as indicated by $\beta = 1$.

One can see in Figure 2 a noticeable difference in the concentration profiles and output current when the diffusion modules, σ_1^2 and σ_2^2, or the maximal enzymatic rates, V_1 and V_2, are varied. The steady-state current density I_{ss} varies by several orders of magnitude, ranging from 0.66 to 36.7 $\mu\text{A/cm}^2$. However, the sum of the steady-state concentrations at any spatial point remains constant and equals θS_0 in the enzyme layer and S_0 in the diffusion layer, as determined in (17) and (18). Although the steady-state current density I_{ss}

differs by nearly an order of magnitude (Figure 2d), the dynamics of the biosensor response are similar, as the half-time $T_{0.5}$ varies only slightly, from 2.0 s to 2.2 s.

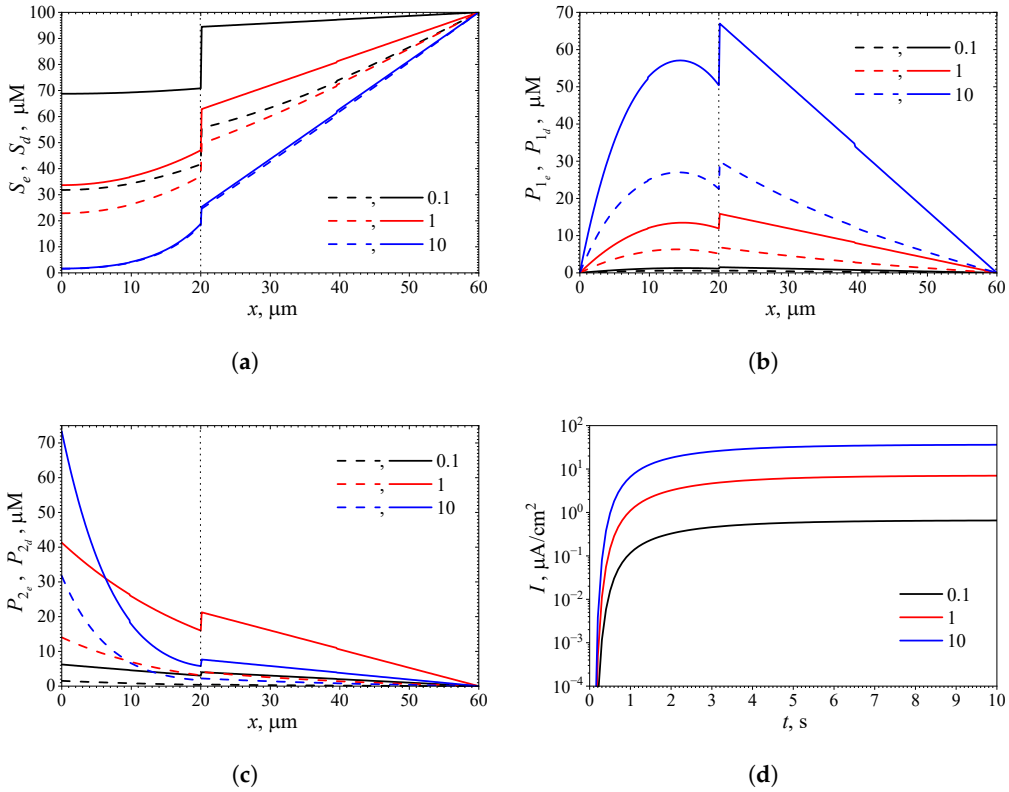


Figure 2. Steady-state (solid lines) and half-time ($T_{0.5}$, dashed lines) concentration profiles of the substrate S (**a**), product P_1 (**b**), and product P_2 (**c**), as well as the evolution of the current density I (**d**), simulated at $\kappa = 1$ ($K_2 = K_1$), $\beta = 1$ ($\theta = 0.75$), for three values of diffusion modules σ_1^2 and σ_2^2: 0.1, 1, and 10. Other parameters are as defined in (34). Dotted lines indicate the boundary between the enzyme and diffusion layers.

As far as is known from the literature, the steady-state concentrations at the electrode surface ($x = 0$) are somewhat unexpected, since a zero substrate concentration has been reported there [27,35,37]. Figure 2 shows that this occurs only when internal diffusion limitation is present ($\sigma_1^2 \gg 1$). Note that the substrate is unaffected by the activity of the second enzyme, so the substrate dynamics have been extensively studied [11,26,38,42,43]. Nevertheless, unjustified assumptions regarding the steady-state concentrations at the electrode surface have sometimes been introduced, even when deriving analytical steady-state solutions for biosensors exhibiting the CEC mechanism [37].

According to (23a), for a first-order reaction rate R_1, the steady-state substrate concentration approaches its maximum value of θS_0 as $\alpha_1 \to 0$ (or equivalently, as $\sigma_1 \to 0$). It decreases rapidly with increasing α_1 as well as σ_1, since $\sigma_1 = d_e\alpha_1$. In particular, $S_{ess}(0) \approx 0.37\theta S_0$ at $\sigma_1 = 1$, and $S_{ess}(0) \approx 8.25 \times 10^{-6}\theta S_0$ at $\sigma_1 = 10$. For a zero-order reaction rate, the steady-state substrate concentration defined in (29a) also approaches its maximum value of θS_0 as $\alpha_1 \to 0$.

4.2. Effect of Internal Diffusion Limitations

To assess the impact of internal diffusion limitations on the biosensor response, simulations were performed over a broad range of maximal enzymatic rates, V_1 and V_2, while all other parameters were kept identical to those used in the simulations presented in Figure 2. This approach allowed for observation of the transition from enzyme-kinetic

control ($\sigma_1^2 \ll 1$ and $\sigma_2^2 \ll 1$) to complete internal-diffusion control ($\sigma_1^2 \gg 1$ and $\sigma_2^2 \gg 1$) to be observed [3,11,42,48,72].

In the simulations, the maximal enzymatic rates V_1 and V_2 were varied across four orders of magnitude, ranging from 1 μM/s to 10 mM/s. The calculations assumed comparable mass transport in the outer diffusion layer and the enzyme layer (d_d = 40 μm, β = 1, θ = 0.75), as well as identical Michaelis constants ($K_2 = K_1$, $\kappa = 1$).

Although only the maximal enzymatic rates were varied in these simulations, the results remain applicable for a wider range of model parameters, since each diffusion module σ_i^2 incorporates four parameters of the model: the diffusion coefficient D_e in the enzyme layer (introduced in (20)); the enzyme layer thickness d_e; the Michaelis constant K_i; and the maximal enzymatic rate V_i, $i = 1, 2$. Analyzing biosensor performance in terms of dimensionless parameters removes dependence on specific units and experimental scales, thereby enabling broader generalization of the results [40,41,60]. Figure 3 shows the dependence of the dimensionless biosensor characteristics on the diffusion modules σ_1^2 and σ_2^2.

One can see in Figure 3a that the dimensionless steady-state output current I_{ss}^* is a monotonically increasing function of both diffusion modules, σ_1^2 and σ_2^2, as well as of the maximal enzymatic rates V_1 and V_2. The application of the active enzyme E_2 ($V_2 > 0$, $\sigma_2^2 > 0$) causes a severalfold increase in the biosensor current. However, Figure 3e shows that this increase adversely affects the response dynamics, as it prolongs the half-time $T_{0.5}^*$ by severalfold.

The largest signal gain (G = 19.8, Figure 3b) occurs at the lowest activity of enzyme E_1 ($\sigma_1^2 = 0.01$) and the highest activity of enzyme E_2 ($\sigma_2^2 = 100$), when the biosensor operates the slowest, as indicated by the largest half-time ($T_{0.5}^*$ = 3.4). A slightly lower gain (G = 16.4) is obtained when the biosensor response is governed primarily by internal diffusion limitation ($\sigma_1^2 = 100$, $\sigma_2^2 = 100$), in which case the half-time is also smaller ($T_{0.5}^*$ = 2.0). This biosensor configuration is attractive also because of its relatively high sensitivity (B_s^* = 0.85, Figure 3c) and broad linear range of its calibration curve (K_{app}^* = 54.7).

Let us compare the gain, simulated for a mean substrate concentration $S_0 = K_1 = K_2$, shown in Figure 3b, with the analytical expressions obtained for first- and zero-order reaction rates,

$$G_1 = \sigma_2 \mathcal{B} \frac{1+\beta}{\beta}, \quad G_0 = 1 + \frac{\sigma_2^2}{\sigma_1^2}\kappa, \tag{35}$$

where G_1 is the gain under first-order conditions, derived using (27), and G_0 is the gain under zero-order conditions, derived using (32). The gain G_1 does not depend on the rate of the first enzymatic reaction and is approximately 20 when evaluated at $\sigma_2^2 = 100$ and $\beta = 1$, for which $\mathcal{B} \approx 1$. The simulated gain $G = 19.8$ at these parameter values and $\sigma_1^2 = 0.01$ (Figure 3b) is comparable with G_1. However, the gain under transition conditions decreases slightly with increasing σ_1^2, which is expected because under the zero-order conditions, the gain G_0 depends explicitly on σ_1^2.

Figure 3 shows that an increase in the diffusion module σ_2^2 (i.e., an increase in enzyme E_2 activity) leads to an increase in the dimensionless steady-state current I_{ss}^*, half-time $T_{0.5}^*$, and signal gain G but to a slight decrease in the sensitivity B_s^* and apparent Michaelis constant K_{app}^*.

The complex nature of biosensors requires the simultaneous optimization of multiple, often conflicting, objectives, meaning that improving one may lead to the deterioration of others [29,31]. Multi-objective optimization, combined with multi-dimensional visualization, can be employed to identify trade-off solutions and support decision-making in biosensor design [30].

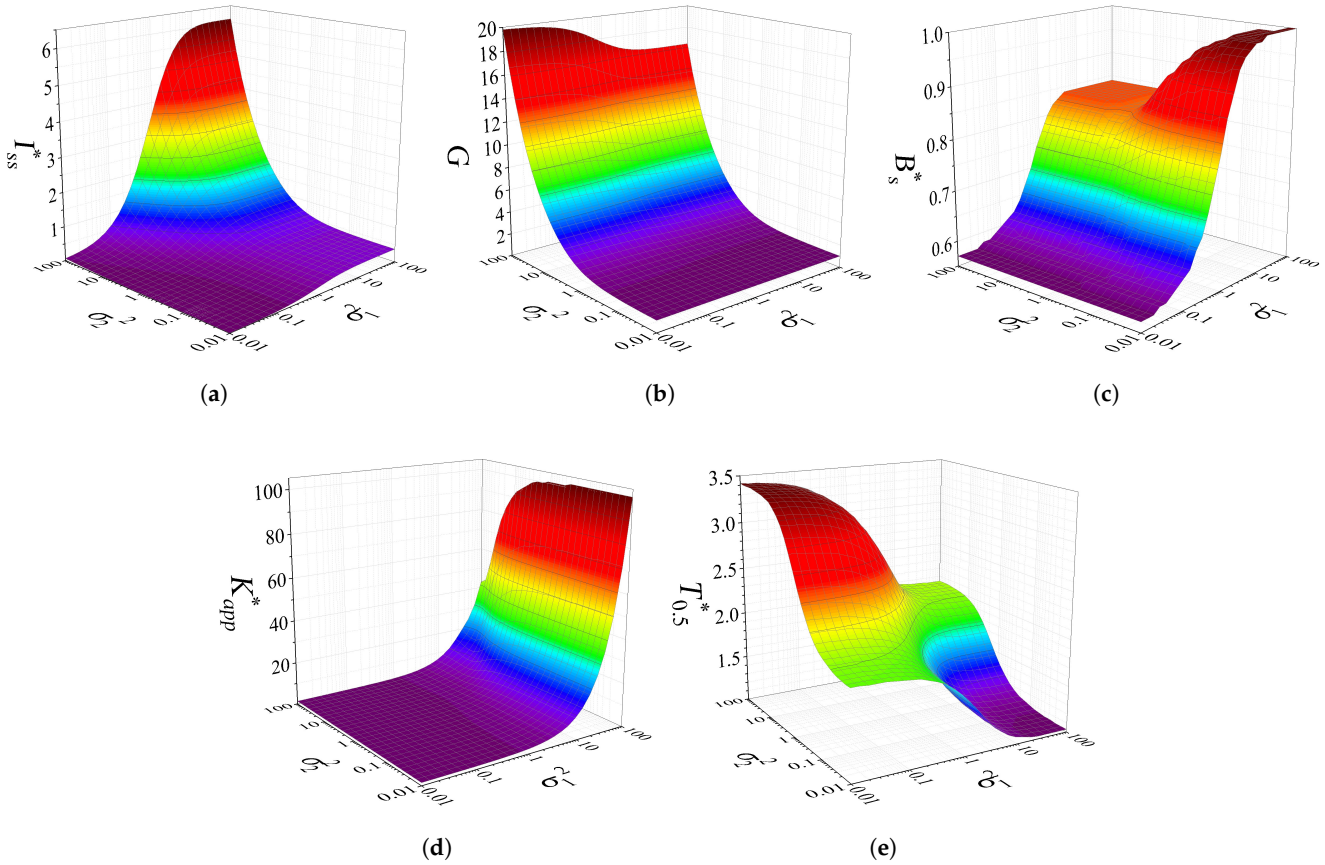


Figure 3. Dimensionless steady-state current I^*_{ss} (**a**), signal gain G (**b**), sensitivity B^*_s (**c**), apparent Michaelis constant K^*_{app} (**d**), and half-time $T^*_{0.5}$ (**e**) as functions of the diffusion modules σ_1^2 and σ_2^2, simulated at $\kappa = 1$ and $\beta = 1$. The other parameters are as defined in (34).

Similar dependencies of the signal gain and sensitivity on the dimensional maximal enzymatic rates and enzyme layer thickness were also observed in previously reported one- and two-layer mathematical models of CEC biosensors [26,27,37]. Particularly, Coche-Guerente et al. reported that the CEC biosensor sensitivity increases with enzyme layer thickness up to a limiting value [26]. Figure 3c similarly demonstrates the emergence of a limiting sensitivity as both diffusion modules (in particular, the enzyme layer thickness) increase. However, this limiting value is reached non-monotonically when $\sigma_1^2 > 1$. The limiting value of the dimensional sensitivity B_s was computationally determined by Coche-Guerente et al. for low substrate concentrations, that is, for first-order reaction rates. The sensitivity for the linear cases of the model in (3)–(8) can be analyzed analytically using the expressions (27) and (32) for the steady-state current. In particular, the sensitivity under first-order conditions is given by the following:

$$B_s = n_e F \theta \frac{D_e}{d_e}\left(1 - \frac{1}{\mathcal{A}}\right)\sigma_2 \mathcal{B}, \tag{36a}$$

$$\lim_{d_e \to \infty} B_s = n_e F \theta D_e \alpha_2, \quad S_0 \ll K_1, S_0 \ll K_2\,. \tag{36b}$$

The limiting value defined in (36b) is invariant with respect to external mass transfer by diffusion, as was also determined by Coche-Guerente et al. for specific model parameter values [26]. Further analysis of (36a) indicates that the limiting value of the sensitivity B_s is reached non-monotonically at large enzyme layer thicknesses d_e. The sensitivity B_s is a

monotonically increasing function of d_e when the diffusion layer thickness d_d approaches zero ($\beta \to \infty$).

Figure 3e shows that the dimensionless half-time $T^*_{0.5}$ is approximately 2 for all examined cases with equal diffusion modules, i.e., when $\sigma_1^2 = \sigma_2^2$. The value of $T^*_{0.5}$ decreases noticeably with increasing ratio σ_1^2/σ_2^2, and increases in the opposite case.

Substrate concentration also contributes to the monotonicity observed in CEC biosensor sensitivity. Salomi et al. demonstrated that the dimensionless sensitivity of a CEC biosensor varies non-monotonically with the substrate concentration S_0, exhibiting a local minimum near the characteristic concentration $S_0 = K_1 = K_2$, where the biosensor kinetics within the enzyme layer transition from first- to zero-order [37]. Nevertheless, the dimensional (B_s) and dimensionless (B^*_s) sensitivities approach zero under zero-order reaction conditions ($S_0 \gg K_1$ and $S_0 \gg K_2$), because the steady-state current I_{ss} becomes independent of S_0, as predicted by the analytical expression (32). Figure 3c further shows that B^*_s is also a non-monotonic function of σ_1^2 at the mean substrate concentration when $\sigma_2^2 > 10$.

The dependence of the steady-state current I^*_{ss} and the gain G on the diffusion modules σ_1^2 and σ_2^2, under conditions where mass transport in the outer diffusion layer is comparable to that in the enzyme layer (β = 1, θ = 0.75), as shown in Figure 3, is very similar to that obtained in a computational study neglecting outer diffusion effects [27]. For example, at $\sigma_2^2 = 100$, G varies approximately between 15 to 17 when outer diffusion limitations are ignored [27], whereas it ranges from 16.4 to 19.8 for β = 1 (Figure 3b).

An increase in signal gain and sensitivity, similar to that shown in Figure 3b,c, was also experimentally observed for an amperometric enzyme electrode with immobilized laccase, in which chemical amplification through cyclic substrate conversion occurs within a single enzyme membrane [77].

4.3. Effects of External Diffusion Limitations

The dimensionless Biot number, which compares the relative external and internal transport resistances, is widely used to assess the impact of external mass transfer limitations [9,42,48,54,71]. Considering the definition of the Biot number β given in (15), the influence of external diffusion limitations on the CEC biosensor response was examined by simulating the sensor behavior while varying the thickness d_d of the external diffusion layer from 2 µm to 400 µm. This range ensured that β varied over two orders of magnitude, from 20 to 0.1. The simulations were carried out assuming identical diffusion modules and Michaelis constants ($\sigma_1^2 = \sigma_2^2 = \sigma^2$, $K_1 = K_2$, $\kappa = 1$), with the partition coefficient fixed at $\theta = 0.75$. The simulation results are shown in Figure 4.

Figure 4a shows that the steady-state current I^*_{ss} is practically invariant to external diffusion limitations, as characterized by the Biot number β, while the partitioning remains constant. Only when the reactions inside the enzyme layer are relatively slow ($\sigma^2 < 1$) does I^*_{ss} slightly increase when increasing the limitation of outer mass transport (decreasing β). In particular, at $\sigma^2 = 0.01$, I^*_{ss}, which remains at a low level, increases from 2.3×10^{-3} to 4.4×10^{-3} as β decreases from 20 to 0.1.

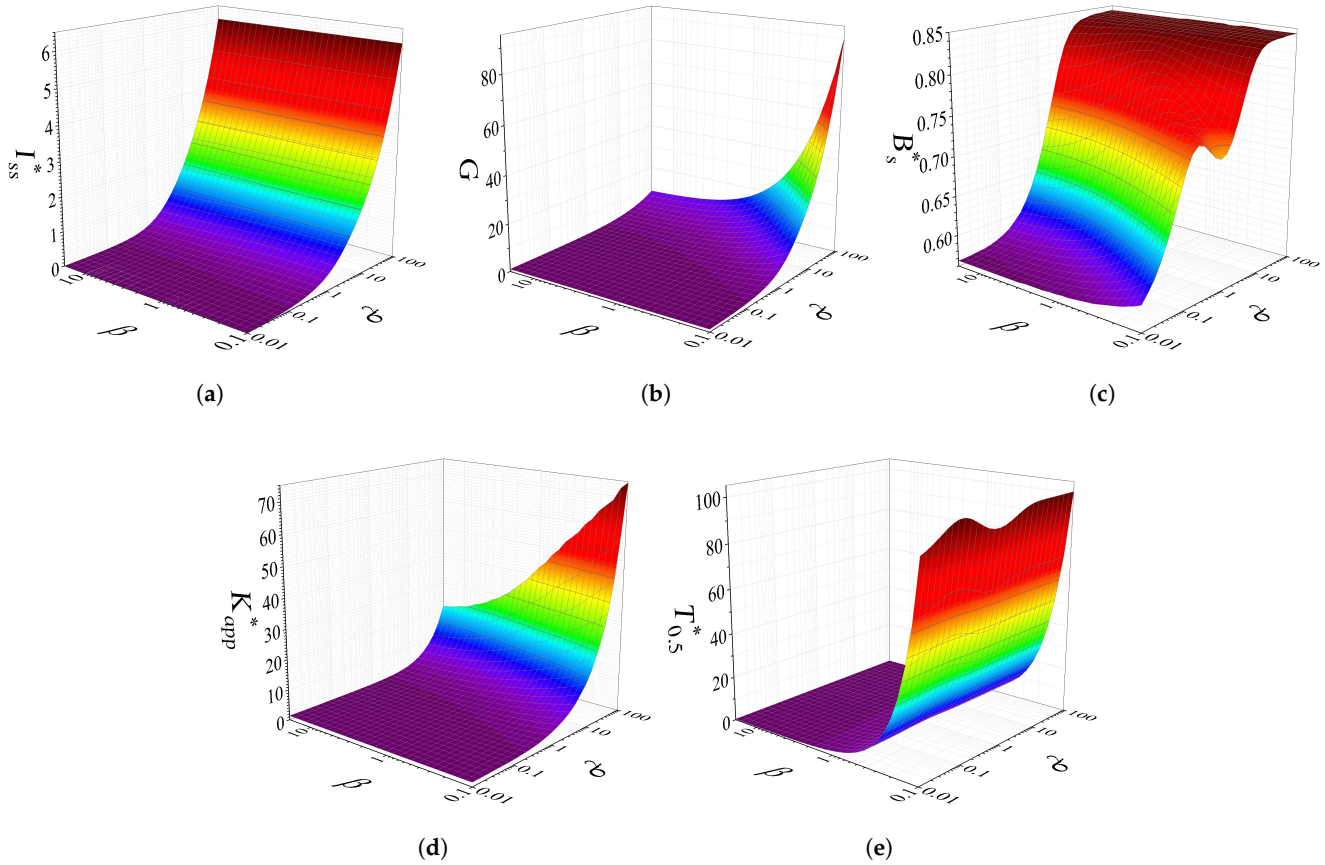


Figure 4. Dimensionless steady-state current I_{ss}^{*} (**a**), signal gain G (**b**), sensitivity B_{s}^{*} (**c**), apparent Michaelis constant K_{app}^{*} (**d**), and half-time $T_{0.5}^{*}$ (**e**) as functions of the Biot number β and the diffusion module $\sigma^2 = \sigma_1^2 = \sigma_2^2$, assuming $\kappa = 1$ and $\theta = 0.75$. The other parameters are as defined in (34).

In conventional mono-enzyme biosensors operating under the CE scheme, increased external diffusion resistance (decreased β) is typically associated with a reduction in output current [9,42,49,50,54]. However, in the present CEC amplification system, the observed behavior arises from a fundamentally different mechanism [22,26].

Within our model, decreasing the diffusion parameter β at a fixed value of σ^2 increases the residence time of the electrochemically generated product P_2 within the enzymatic region. This enhanced confinement favors its enzymatic reconversion to P_1 rather than allowing it to diffuse into the bulk solution. As a result, the efficiency of the catalytic cycling between P_1 and P_2 is increased, leading to a higher steady-state current I_{ss}^{*} and signal gain G. Thus, under these conditions, diffusion limitation does not suppress the current but instead enhances enzymatic amplification by reducing the loss of intermediates involved in the CEC cycle [22,23,26].

For $\sigma^2 \gg 1$, the system enters an internal diffusion-dominated regime, in which enzymatic turnover within the enzyme layer is much faster than diffusive transport. The electrochemically generated intermediate P_2 is therefore rapidly reconverted within the enzyme layer, minimizing its loss to the bulk solution. As a consequence, catalytic cycling between P_1 and P_2 becomes highly efficient, and the steady-state current is governed primarily by enzymatic kinetics rather than by external mass transport, rendering it effectively invariant to the diffusion parameter β. The same effect of external diffusion resistance for $\sigma^2 \gg 1$ has also been observed in amperometric biosensors with substrate cyclic conversion [45].

Keeping the unchanged output current while increasing the external diffusion resistance leads to an increase in signal gain, as shown in Figure 4b. At $\sigma^2 = 100$, the signal gain G increases from 8.6 to 90.3, while the steady-state current stagnates.

Maintaining an essentially unchanged output current while increasing the external diffusion resistance results in a pronounced increase in signal gain, as shown in Figure 4b. At $\sigma^2 = 100$, the signal gain G increases by a factor of 10.9 (from 8.6 to 90.3) solely as a result of enhanced limitation of outer mass transport.

The gain G_1, derived for first-order kinetics and given in (35), is also applicable under the assumption $\sigma_1 = \sigma_2 = \sigma$, as adopted in simulations shown in Figure 4. For $\sigma^2 = 100$, G_1 increases monotonically from 10.5 to 110 as the Biot number β decreases from 20 to 0.1, whereas the gain G obtained under transition conditions (Figure 4b) increases from 8.6 to 90.3 over the same range. This reduction in gain is expected, since the corresponding zero-order gain G_0 is relatively small, $G_0 = 1 + \kappa = 2$.

A relatively strong limitation of outer mass transport, characterized by $\beta = 0.1$ and yielding the largest signal gain G, occurs at a comparatively large diffusion layer thickness of $d_d = 300\,\mu\text{m}$, assuming $\theta = 1$ (i.e., perfect contact conditions), while the remaining parameters are taken from (34). This external diffusion limitation can also be introduced by applying a semi-permeable, diffusion-limiting membrane onto the enzyme layer [33,40,42]. Such a membrane can provide external mass-transfer resistance corresponding to $D_d/d_d = 2\,\mu\text{m/s}$, for example by using a thin ($d_d \approx 3\,\mu\text{m}$) biocompatible membrane composed of two medical-grade polyurethanes and developed for highly sensitive glucose biosensors, which has a diffusivity of $D_d = 0.67\,\mu\text{m}^2/\text{s}$ [67].

One can observe in Figure 4c a nonmonotonic dependence of the sensitivity B_s^* on σ^2 for $\beta \lesssim 0.2$, whereas at higher values of β, the sensitivity B_s^* increases monotonically with increasing σ^2. A similar nonmonotonic behavior is also observed for the biosensor response time ($T_{0.5}^*$, Figure 4e). This nonmonotonicity arises under relatively strong external diffusion limitations ($\beta \lesssim 0.2$), when the control of the biosensor response shifts from enzyme kinetics to internal diffusion limitation (i.e., when $0.1 \lesssim \sigma^2 \lesssim 10$).

Figure 4c also shows that the dependence of the sensitivity B_s^* on β is generally weak. For $\sigma^2 \lesssim 0.3$, B_s^* increases slightly with decreasing β. For example, at $\sigma^2 = 0.01$, the sensitivity B_s^* increases from 0.56 to 0.59 as the outer diffusion limitation becomes stronger (i.e., as β decreases from 20 to 0.1). By contrast, at $\sigma^2 = 100$, the sensitivity is practically independent of the outer diffusion limitation, with $B_s^* \approx 8.4$. At intermediate values of σ^2, B_s^* exhibits a weakly nonmonotonic dependence on β.

A similar dependence of the sensitivity on the outer diffusion limitation, including a slight increase in sensitivity with increasing outer diffusion layer thickness (i.e., with increasing outer diffusion limitation, or equivalently, decreasing β) was previously observed by Coche-Guerente et al., when the rotation rate of the catechol–polyphenol oxidase-based bioelectrode decreased [26].

In the simulations presented in Figure 4, the diffusion modules σ_1^2 and σ_2^2 were assumed to be identical ($\sigma^2 = \sigma_1^2 = \sigma_2^2$). Under this assumption, the expression (36a) for the sensitivity B_s, defined for first-order reaction rates, was simplified as follows:

$$B_s = n_e F \theta \frac{D_e}{d_e} \sigma \frac{\cosh(\sigma) + \sigma \sinh(\sigma)/\beta - 1}{\sinh(\sigma) + \sigma \cosh(\sigma)/\beta}. \tag{37}$$

This expression indicates that B_s increases monotonically with the enzyme layer thickness d_e, as well as with $\alpha = \sigma/d_e$. A similar dependence is valid for the steady-state current I_{ss}.

4.4. Effects of Partitioning

The analytical expressions given in (23a) and (29a) demonstrate that the stationary substrate concentration $S_{e\mathrm{ss}}$ in the enzyme layer depends directly on the product θS_0. Consequently, both at low and very high substrate concentrations, the stationary substrate concentration within the enzyme layer remains unchanged as long as the value of θS_0 is held constant and all other parameters are fixed. Since the partition coefficient θ is added to the definition of the Biot number β, maintaining a constant β requires a corresponding adjustment of either the outer diffusion layer thickness or the diffusion coefficients. This consideration is particularly relevant when the diffusion layer, illustrated in Figure 1, functions as a semi-permeable, porous, or perforated membrane. Such membranes increase the diffusion resistance to the analyte and are commonly employed to retain the enzyme, protect the sensor, and improve both stability and reproducibility of the biosensor response [1,2,16,67].

Since the partition coefficient θ is entered explicitly into expressions for the steady-state concentrations of all species in the enzyme layer and for the output current, and not solely through the Biot number β as defined in (15), the CEC biosensor response was further examined by varying θ over two orders of magnitude, from 0.1 to 10. This variation resulted in a corresponding change in the Biot number β from 7.5 to 0.075, respectively, reflecting a transition from internally to externally dominated mass transfer [9,71]. The diffusion module σ^2 was varied, while all other parameter values were kept identical to those used in the simulations shown in Figure 4, except that the diffusion layer thickness was fixed at $d_d = 40\ \mu\mathrm{m}$. The resulting simulation outcomes are presented in Figure 5.

Figure 5a,b shows that the partitioning effect on the signal gain G is similar to its effect on the steady-state current I_{ss}^*. In particular, when the reactions inside the enzyme layer are fast ($\sigma^2 > 10$), both G and I_{ss}^* increase as the partitioning increases (i.e., as θ increases). At $\sigma^2 = 100$, the signal gain G increases by a factor of 5.2 (from 10.9 to 56.2) solely due to the limitation of outer mass transport. The dimensionless output current I_{ss}^* then increases by as much as 40 times (from 0.95 to 38.8).

The surfaces of the signal gain G and sensitivity B_{s}^* shown in Figure 5 are similar to those presented in Figure 4, since the partition coefficient θ is inversely proportional to the Biot number β, as defined in (15). However, ranges of those biosensor characteristics differ noticeably, even though the ranges of the parameters θ and β are comparable. For example, for σ^2 = 100, the gain G as a function of β attains a maximum value of approximately 90 at $\beta = 0.1$ (Figure 4b). In contrast, the corresponding value of $G \approx 48$ at $\theta = 7.5$ (which corresponds to $\beta = 0.1$) is significantly smaller (Figure 5b). Nevertheless, both stronger outer diffusion limitations (i.e., decreasing β) and enhanced partitioning (i.e., increasing θ) positively affect the signal gain but negatively affect on the response time (i.e., they increase $T_{0.5}^*$, Figures 4e and 5e). However, increasing θ prolongs the response time by noticeably less than decreasing β.

Stronger outer diffusion limitations also prolong the linear range of the calibration curve (i.e., increase K_{app}^*, Figure 4d), whereas enhanced partitioning shortens this range (i.e., decreases K_{app}^*, Figure 5d). This effect is especially pronounced for $\sigma^2 \gtrsim 10$.

The steady-state current I_{ss}^* is considerably more sensitive to partitioning effects than to diffusion limitations (Figures 4a and 5a). For example, at $\sigma^2 = 100$, I_{ss}^* remains approximately constant at 6.1 for all values of β ranging from 0.1 to 20, whereas it decreases markedly from 38.8 to 0.95 as θ is reduced from 10 to 0.1. This pronounced sensitivity of I_{ss}^* to θ arises from the explicit dependence of I_{ss} on θ for first-order reaction rates, as given in (27). By contrast, for zero-order reaction rates, as defined in (32), I_{ss} (and consequently I_{ss}^*) becomes independent of both the substrate concentration S_0 and the partition coefficient θ.

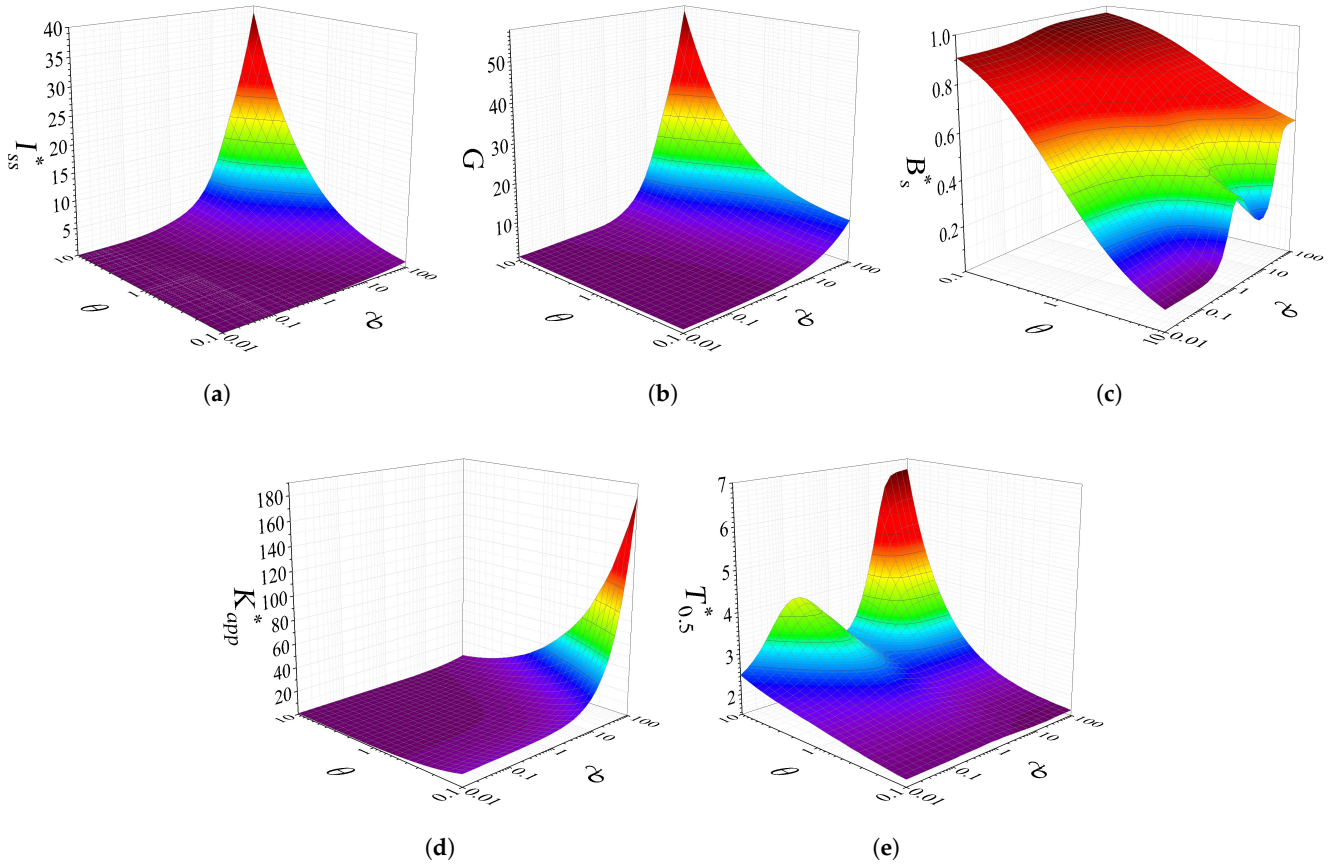


Figure 5. Dimensionless steady-state current I^*_{ss} (**a**), signal gain G (**b**), sensitivity B^*_s (**c**), apparent Michaelis constant K^*_{app} (**d**), and half-time $T^*_{0.5}$ (**e**) as functions of the partition coefficient θ and the diffusion module $\sigma^2 = \sigma_1^2 = \sigma_2^2$, assuming $\kappa = 1$. The other parameters are as defined in (34).

For first-order kinetics ($S_0^* \ll 1$) and sufficiently large values of σ ($\sigma^2 > 10$), the dimensionless steady-state current I^*_{ss} becomes approximately a linear function of σ and θ, such that $I^*_{ss} \approx \theta S_0^* \sigma$. Figure 5a shows that I^*_{ss} also increases approximately linearly with increasing σ and θ under transition conditions, when $S_0^* = 1$. Moreover, under these conditions ($\sigma^2 > 10$) and for constant θ and S_0^*, I^*_{ss} depends linearly only on σ. This behavior can also be observed under transient conditions ($S_0^* = 1$), as shown in Figure 4a.

As shown in Figure 5, the biosensor characteristics exhibit a strong dependence on whether the partition coefficient is large ($\theta > 1$) or small ($\theta < 1$).

In a two-layer amperometric CEC biosensor utilizing reaction scheme (1), a partition coefficient $\theta < 1$ indicates weak accumulation of reaction products P_1 and P_2 within the enzyme layer, leading to reduced residence times, enhanced diffusive losses, and reduced catalytic amplification. In contrast, $\theta > 1$ corresponds to preferential partitioning of these products into the enzyme layer, resulting in higher local concentrations, improved confinement, and more efficient enzymatic cycling between E_1 and E_2, thereby increasing the steady-state current and signal gain [26,32,47,61].

Enzyme-loaded membranes exhibiting $\theta < 1$ are typically based on thin, hydrated polymeric, semipermeable porous (or effectively perforated) matrices that partially exclude the substrate from the membrane phase. In contrast, membranes exhibiting $\theta > 1$ are generally composed of swollen, hydrophobic, or affinity-rich polymeric matrices that preferentially absorb, bind, or solubilize the substrate, resulting in enrichment of the substrate within the membrane relative to the bulk solution [2,3,16,39,47,61].

4.5. Effect of the Ratio for the Michaelis Constants

In the simulations discussed above, the dimensional Michaelis constants, K_1 and K_2, were assumed to be identical, i.e., the ratio $\kappa = K_2/K_1$ was set to unity. This same assumption has also been adopted in most previous studies on trigger biosensors [27,35–38]. Furthermore, the steady-state analytical solutions for both first- and zero-order reaction regimes are explicitly independent of the Michaelis constants, since the expression $\sigma_i^2 K_i$ in the zero-order solution can be rewritten as $V_i d_e^2/D_e$ for $i = 1, 2$. However, the ratio κ is among the dimensionless governing parameters introduced in (15). Although K_1 and K_2 are embedded within the dimensionless diffusion modules σ_1^2 and σ_2^2, their ratio, κ, appears explicitly in the nondimensionalized model (3)–(8) presented in Appendix A. Furthermore, under the first-order conditions, the signal gain G_1 is expressed in (35) as a linear function of κ. Consequently, κ can influence the behavior of the CEC biosensor.

To investigate the effect of the ratio, κ, of the Michaelis constants on the CEC biosensor response, the response was simulated by varying the Michaelis constant K_2 over two orders of magnitude, from $0.1K_1$ to $10K_1$. The effect of κ was studied by independently varying the diffusion module σ^2 from 0.01 to 100, under the assumption that $\sigma^2 = \sigma_1^2 = \sigma_2^2$. Changes in K_2 at a given value of σ^2 resulted in corresponding adjustment of V_2 to maintain the constraint $\sigma_2^2 = \sigma_1^2$ in all simulations.

In addition, the influence of κ on the CEC biosensor response was investigated under various external diffusion limitations and partitioning conditions, assuming $\sigma^2 = \sigma_1^2 = \sigma_2^2 = 1$. The sensor responses were simulated by independently varying the Biot number β from 0.1 to 20 and the partition coefficient θ from 0.1 to 1. Variations in β were achieved by adjusting the thickness d_d of the external diffusion layer while keeping $\theta = 0.75$ constant. Conversely, variations in θ were performed at a fixed external diffusion layer thickness of $d_d = 40$ μm. The simulation results are presented in Figures 6–8.

Figures 6–8 demonstrate that the ratio κ of the Michaelis constants has a significant impact on the biosensor response, particularly when the analytical system is internally diffusion-limited ($\sigma_2^2 > 1$ and $\sigma_1^2 > 1$, Figure 6) or externally diffusion-limited ($\beta < 1$, Figure 7; $\theta > 1$, Figure 8). Under these conditions, increasing κ leads to an increase in the steady-state current I_{ss}^* and signal gain G. However, this improvement is accompanied by an undesired increase in the response time $T_{0.5}^*$.

The output current and gain of a CEC biosensor involving an enzyme E_1 with a higher substrate affinity than another enzyme E_2 ($K_1 < K_2$, $\kappa > 1$) are greater than those of the corresponding biosensor in which E_1 has a lower affinity than E_2 ($\kappa < 1$), when both biosensors operate under identical internal or external diffusion-limited conditions (Figures 6 and 7). In particular, under strong internal diffusion limitation of $\sigma^2 = 100$, the dimensionless current I_{ss}^* and gain G are 2.2 times higher, and sensitivity B_s is 1.6 times higher at $\kappa = 10$ than at $\kappa = 0.1$ (Figure 6a–c). However, at the same time, the linear range of the calibration curve (K_{app}^*) becomes slightly narrower, and the response time ($T_{0.5}^*$) increases (Figure 6d,e).

The biosensor sensitivity B_s^* increases monotonically with κ when $\sigma^2 > 1$ (Figure 6c) or $\beta < 1$ (Figure 7c). In contrast, for $\theta > 1$, B_s^* exhibits a minimum at $\kappa = 1$ (Figure 8c). Similarly, for $\sigma^2 > 1$ (Figure 6d) and $\beta < 1$ (Figure 7d), the apparent Michaelis constant K_{app}^* also exhibits a minimum at $\kappa = 1$.

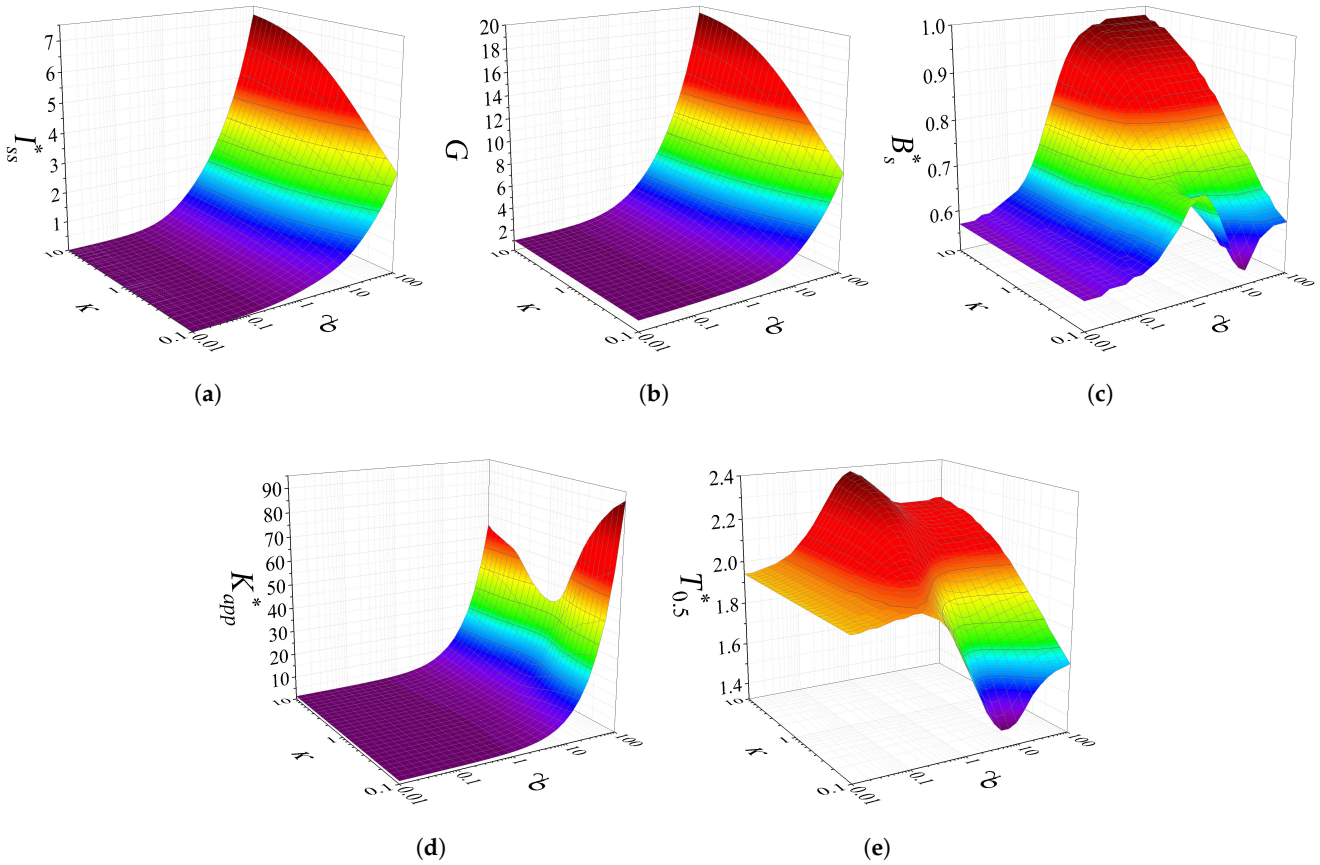


Figure 6. Dimensionless steady-state current I^*_{ss} (**a**), signal gain G (**b**), sensitivity B^*_s (**c**), apparent Michaelis constant K^*_{app} (**d**), and half-time $T^*_{0.5}$ (**e**) as functions of the ratio κ of the Michaelis constants and the diffusion module σ^2. Simulations were performed at $\beta = 1$ and $\theta = 0.75$, assuming $\sigma^2 = \sigma_1^2 = \sigma_2^2$. The other parameters are as defined in (34).

Figures 7a,b shows that under external diffusion-limited conditions ($\sigma^2 = 1$ and $\beta = 0.1$), both the dimensionless steady-state current I^*_{ss} and the gain G are approximately 3.7 times higher at $\kappa = 10$ than at $\kappa = 0.1$. At the same time, the sensitivity B^*_s increases by nearly a factor of two, from 0.51 to 0.96, whereas the apparent constant K^*_{app} deceases slightly, from 7.3 to 6.3 (Figure 7d). Notably, K^*_{app} reaches a minimum value of approximately 4 at $\kappa \approx 1$ (Figure 7d). The time ($T^*_{0.5}$) then increases by a factor of 2.1 (Figure 7e).

Figure 8 shows that, over a range of values of the Michaelis constant ratio κ, the partition coefficient θ influences the characteristics of the CEC biosensor even more strongly than the Biot number β (Figure 7). In particular, for the partitioning corresponding to $\theta = 10$, the steady-state current I^*_{ss} and the gain G at $\kappa = 10$ are approximately 6.7 times higher than those at $\kappa = 0.1$. However, this enhancement is accompanied by an undesirable increase in the response time $T^*_{0.5}$ by a factor of 4.9.

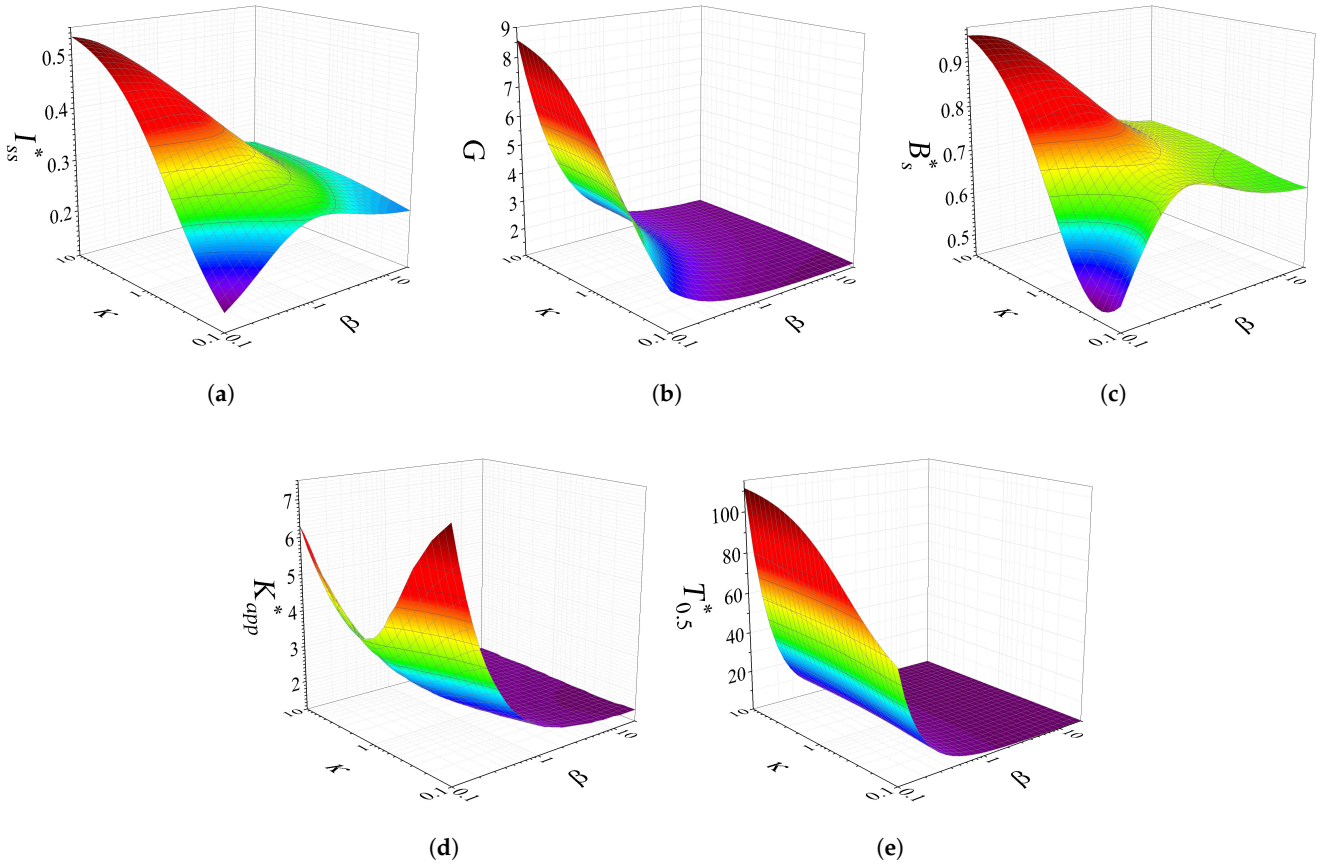


Figure 7. Dimensionless steady-state current I_{ss}^* (**a**), signal gain G (**b**), sensitivity B_s^* (**c**), apparent Michaelis constant K_{app}^* (**d**), and half-time $T_{0.5}^*$ (**e**) as functions of the ratio κ of the Michaelis constants and the Biot number β. Simulations were performed at $\theta = 0.75$ and $\sigma_1^2 = \sigma_2^2 = 1$. The other parameters are as defined in (34).

Such a strong influence of partitioning on the biosensor behavior can be explained by the appearance of the partition coefficient θ in the definition of the Biot number β, as given in (15). An increase in θ leads to a decrease in β when all other model parameters are fixed, thereby enhancing external diffusion limitations and amplifying the overall effect of partitioning. Notably, the Biot number β is a model-dependent dimensionless group rather than a fundamental constant. When equilibrium partitioning occurs at the interface, the resistance ratio necessarily involves θ [41,71].

The constraint $\sigma_1^2 = \sigma_2^2$ for two enzymes, E_1 and E_2, with different substrate affinities ($K_1 \neq K_2$), can be maintained by adjusting the maximal enzymatic rates, V_1 and V_2. A specific value of the maximal enzymatic rate V_i can be achieved by selecting an appropriate concentration of enzyme E_i, since V_i is directly proportional to the enzyme concentration according to $V_i = k_{cat_i} E_{i0}$, where k_{cat_i} is the catalytic rate constant and E_{i0} is the total concentration of E_i ($i = 1, 2$) [3,4].

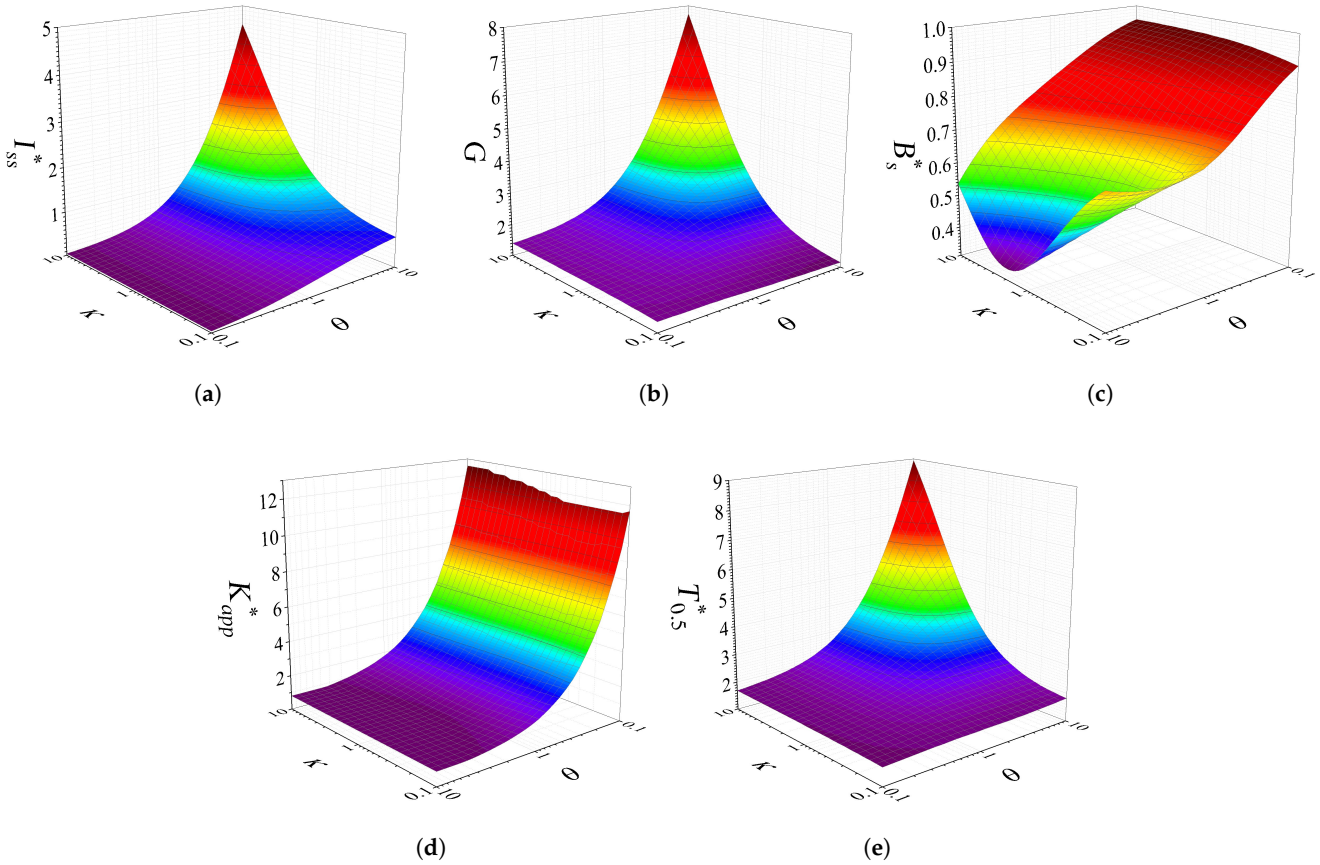


Figure 8. Dimensionless steady-state current I_{ss}^* (**a**), signal gain G (**b**), sensitivity B_s^* (**c**), apparent Michaelis constant K_{app}^* (**d**), and half-time $T_{0.5}^*$ (**e**) as functions of the ratio κ of the Michaelis constants and the partition coefficient θ. Simulations were performed at $\sigma_1^2 = \sigma_2^2 = 1$. The other parameters are as defined in (34).

5. Conclusions

The two-compartment mathematical model in (3)–(9), which describes amperometric bienzyme biosensors (Figure 1) employing an enzymatic trigger reaction (1), provides a useful framework for analyzing the effects of enzymatic kinetics, diffusion limitations, and partitioning on signal amplification and sensor sensitivity, and it enables biosensor design parameters to be optimized. Derivation of the corresponding dimensionless form (A1)–(A6) highlights the key governing dimensionless parameters (15).

An increase in the activity of enzyme E_2, which catalyzes the cyclic product conversion (i.e., an increase in the diffusion module σ_2^2), results in a higher dimensionless steady-state current I_{ss}^* and signal gain G but causes a slight decrease in the sensitivity B_s^*, apparent Michaelis constant K_{app}^*, and overall performance. The largest signal gain is achieved at the lowest activity of enzyme E_1 ($\sigma_1^2 = 0.01$) and the highest activity of enzyme E_2 ($\sigma_2^2 = 100$); however, under these conditions, the biosensor operates the slowest (Figure 3).

When both enzymatic reactions within the enzyme layer are very fast ($\sigma_1^2 > 10$ and $\sigma_2^2 > 10$), the introduction of additional mass transport resistance to the surrounding layer (i.e., decreasing β) leads to a pronounced increase in the signal gain G. In particular, at $\sigma^2 = 100$, G increases by a factor of 10.9 solely due to the limitation of external mass transport, while the steady-state output current I_{ss}^* remains practically unchanged (Figure 4). Furthermore, increasing the partitioning enhances both the signal gain G and the steady-state current I_{ss}^*, especially when the partition coefficient θ exceeds unity, although it adversely affects the response time (Figure 5).

The ratio κ of the Michaelis constants K_2 and K_1 significantly affects the biosensor response, particularly when the analytical system is internally ($\sigma_1^2 = \sigma_2^2 > 10$, Figure 6) or externally ($\beta < 1$, Figure 7) diffusion-limited. The steady-state current and the signal gain of a CEC biosensor involving an enzyme E_1 with a higher substrate affinity than another enzyme E_2 ($K_2 = 10K_1$, $\kappa = 10$) can be several times greater than those of the corresponding biosensor in which E_1 has a lower affinity than E_2 ($K_2 = 0.1K_1$, $\kappa = 0.1$), when both biosensors operate under identical internal or external diffusion-limited conditions. Preferential substrate partitioning into the enzyme layer ($\theta > 1$) further enhances the biosensor performance (Figure 8). However, this enhancement is accompanied by an increase in the response time (Figures 6e, 7e and 8e).

The results presented in this work are restricted to the assumption of species-independent diffusion and partition coefficients, as defined in (20). In practical systems, however, different chemical species may exhibit distinct diffusion coefficients and partitioning behaviors. Extending the present framework to account for species-specific transport parameters represents a direction for future studies and may further improve the quantitative accuracy and predictive capability of the model.

The complex nature of CEC biosensors necessitates the simultaneous optimization of multiple performance objectives, as improvements in certain parameters may lead to the deterioration of others (Figures 3–7). Multi-objective optimization, coupled with multi-dimensional visualization techniques, can be employed to identify trade-off solutions and facilitate informed decision-making in biosensor design.

Author Contributions: Conceptualization, R.B.; methodology, R.B.; software, R.B.; validation, R.B. and K.P.; formal analysis, R.B. and K.P.; investigation, R.B. and K.P.; resources, R.B. and K.P.; data curation, R.B.; writing—original draft preparation, R.B.; writing—review and editing, R.B. and K.P.; visualization, R.B.; supervision, R.B. All authors have read and agreed to the published version of the manuscript.

Funding: This research received no external funding.

Institutional Review Board Statement: Not applicable.

Informed Consent Statement: Not applicable.

Data Availability Statement: No external data were used in this study. All data were generated through computer simulations as described in the article.

Acknowledgments: The authors sincerely thank Juozas Kulys and Feliksas Ivanauskas for their valuable discussions and contributions to the biosensor modeling.

Conflicts of Interest: The authors declare no conflicts of interest.

Abbreviations

The following abbreviations are used in this manuscript:

S	Substrate
E_i	The *i*th enzyme
P_i	The *i*th reaction product
QSSA	Quasi-steady-state approximation
CEC	Catalytic–electrochemical–catalytic mechanism
CE	Catalytic–electrochemical mechanism

Appendix A. Nondimensionalized Mathematical Model

The two-compartment model (3)–(8) was nondimensionalized by rescaling the time, space, concentrations, and diffusion coefficients as defined in Table A1.

The resulting dimensionless governing Equations (3) and (4) can thus be expressed for $t^* > 0$ as follows:

$$\frac{1}{\eta_{S_e}}\frac{\partial S_e^*}{\partial t^*} = \frac{\partial^2 S_e^*}{\partial x^{*2}} - \sigma_1^2 \frac{S_e^*}{1+S_e^*}, \tag{A1a}$$

$$\frac{1}{\eta_{P_{1e}}}\frac{\partial P_{1e}^*}{\partial t^*} = \frac{\partial^2 P_{1e}^*}{\partial x^{*2}} + \frac{\eta_{S_e}}{\eta_{P_{1e}}}\sigma_1^2 \frac{S_e^*}{1+S_e^*} + \kappa \frac{\eta_{P_{2e}}}{\eta_{P_{1e}}}\sigma_2^2 \frac{P_{2e}^*}{1+P_{2e}^*}, \tag{A1b}$$

$$\frac{1}{\eta_{P_{2e}}}\frac{\partial P_{2e}^*}{\partial t^*} = \frac{\partial^2 P_{2e}^*}{\partial x^{*2}} - \sigma_2^2 \frac{P_{2e}^*}{1+P_{2e}^*}, \quad x^* \in (0,\, 1), \tag{A1c}$$

where $\eta_{S_e} = D_{S_e}/D_{\text{ref}}$ and $\eta_{P_{ie}} = D_{P_{ie}}/D_{\text{ref}}$ are the dimensionless diffusivity ratios for the substrate and products in the enzyme layer.

The system of diffusion Equation (4) can be expressed in the following form for $t^* > 0$:

$$\frac{\partial S_d^*}{\partial t^*} = \eta_{S_d}\frac{\partial^2 S_d^*}{\partial x^{*2}}, \tag{A2a}$$

$$\frac{\partial P_{1d}^*}{\partial t^*} = \eta_{P_{1d}}\frac{\partial^2 P_{1d}}{\partial x^{*2}}, \tag{A2b}$$

$$\frac{\partial P_{2d}^*}{\partial t^*} = \eta_{P_{2d}}\frac{\partial^2 P_{2d}}{\partial x^{*2}}, \quad x \in (1,\, a_2^*), \tag{A2c}$$

where $\eta_{S_d} = D_{S_d}/D_{\text{ref}}$ and $\eta_{P_{id}} = D_{P_{id}}/D_{\text{ref}}$ are the dimensionless diffusivity ratios for the substrate and products in the diffusion layer, and $a_2^* = a_2/a_1$ is the dimensionless thickness of the diffusion layer.

The initial conditions given in (5) can be expressed as follows:

$$S_e^*(x^*,0) = 0,\ x^* \in [0,\,1]; \quad S_d^*(x^*,0) = 0,\ x^* \in [1, a_2^*); \quad S_d^*(a_2^*,\,0) = S_0^*, \tag{A3a}$$

$$P_{1e}^*(x^*,0) = 0,\ x^* \in [0,\,1]; \quad P_{1d}^*(x^*,0) = 0,\ x^* \in [1, a_2^*], \tag{A3b}$$

$$P_{2e}^*(x^*,0) = 0,\ x^* \in [0,\,1]; \quad P_{2d}^*(x^*,0) = 0,\ x^* \in [1, a_2^*], \tag{A3c}$$

where S_0^* is the dimensionless substrate concentration in the buffer solution.

The boundary conditions given in (6)–(8) can be expressed as follows ($t^* > 0$):

$$\left.\frac{\partial S_e^*}{\partial x^*}\right|_{x^*=0} = 0, \tag{A4a}$$

$$P_{1e}^*(0,t^*) = 0, \tag{A4b}$$

$$\kappa\,\eta_{P_{2e}}\left.\frac{\partial P_{2e}^*}{\partial x^*}\right|_{x^*=0} = -\eta_{P_{1e}}\left.\frac{\partial P_{1e}^*}{\partial x^*}\right|_{x^*=0}; \tag{A4c}$$

$$S_d^*(a_2^*,t^*) = S_0^*, \tag{A5a}$$

$$P_{id}^*(a_2^*,t^*) = 0, \quad i = 1,2; \tag{A5b}$$

$$\eta_{S_e}\left.\frac{\partial S_e^*}{\partial x^*}\right|_{x^*=1} = \eta_{S_d}\left.\frac{\partial S_d^*}{\partial x^*}\right|_{x^*=1}, \tag{A6a}$$

$$S_e^*(1,t^*) = \theta_S S_d^*(1,t^*), \tag{A6b}$$

$$\eta_{P_{ie}}\left.\frac{\partial P_{ie}^*}{\partial x^*}\right|_{x^*=1} = \eta_{P_{id}}\left.\frac{\partial P_{id}^*}{\partial x^*}\right|_{x^*=1}, \tag{A6c}$$

$$P_{ie}^*(1,t^*) = \theta_{P_i} P_{id}^*(1,t^*). \tag{A6d}$$

Table A1. Dimensional and dimensionless parameters ($i = 1, 2$).

Parameter	Dimensional	Dimensionless
Time	t, s	$t^* = D_{\text{ref}}\, t/a_1^2$
Distance from electrode	x, μm	$x^* = x/a_1$
Enzyme layer thickness	d_e, μm	$d_e^* = d_e/a_1 = 1$
Diffusion layer thickness	d_d, μm	$d_d^* = d_d/a_1$
Substrate concentration in enzyme layer	S_e, μM	$S_e^* = S_e/K_1$
Product P_i concentration in enzyme layer	P_{ie}, μM	$P_{ie}^* = P_i/K_i$
Substrate concentration in diffusion layer	S_d, μM	$S_d^* = S_d/K_1$
Product P_i concentration in diffusion layer	P_{id}, μM	$P_{id}^* = P_i/K_i$
Substrate concentration in bulk	S_0, μM	$S_0^* = S_0/K_1$
Michaelis constant for enzyme E_i	K_i, μM	$K_i^* = K_i/K_1$
Apparent Michaelis constant	K_{app}, μM	K_{app}^*
Ratio of Michaelis constants		$\kappa = K_2/K_1$
Maximal enzymatic activity of enzyme E_i	V_i, μM/s	
Current density	I, μA/cm^2	$I^* = Id_e/(n_eFD_{\text{ref}}K_1)$
Biosensor sensitivity	B_s, A/cm^{2}M	$B_s^* = B_sS_0/I_{ss}$
Reference diffusion coefficient	D_{ref}, μm^2/s	
Diffusion coefficient of substrate in enzyme layer	D_{S_e}, μm^2/s	$\eta_{S_e} = D_{S_e}/D_{\text{ref}}$
Diffusion coefficient of product P_i in enzyme layer	$D_{P_{ie}}$, μm^2/s	$\eta_{P_{ie}} = D_{P_{ie}}/D_{\text{ref}}$
Diffusion coefficient of substrate in diffusion layer	D_{S_d}, μm^2/s	$\eta_{S_d} = D_{S_d}/D_{\text{ref}}$
Diffusion coefficient of product P_i in diffusion layer	$D_{P_{id}}$, μm^2/s	$\eta_{P_{id}} = D_{P_{id}}/D_{\text{ref}}$
Diffusivity ratio for substrate in enzyme layer		$\eta_{S_e} = D_{S_e}/D_{\text{ref}}$
Diffusivity ratio for product P_i in enzyme layer		$\eta_{P_{ie}} = D_{P_{ie}}/D_{\text{ref}}$
Diffusivity ratio for substrate in diffusion layer		$\eta_{S_d} = D_{S_e}/D_{\text{ref}}$
Diffusivity ratio for product P_i in diffusion layer		$\eta_{P_{id}} = D_{P_{id}}/D_{\text{ref}}$
Partition coefficient for substrate		θ_S
Partition coefficient for product P_i		θ_{P_i}
Biot number for substrate		$\beta_S = D_{S_d}d_e/(\theta_S D_{S_e}d_d)$
Biot number for product P_i		$\beta_{P_i} = D_{P_{id}}d_e/(\theta_{P_i} D_{P_{ie}}d_d)$
Diffusion module for enzyme E_1		$\sigma_1^2 = V_1d_e^2/(K_1D_{S_e})$
Diffusion module for enzyme E_2		$\sigma_2^2 = V_2d_e^2/(K_2D_{P_{2e}})$

Table A2. Approximate ranges of governing dimensionless parameters.

Parameter	Estimated Range (Refs.)	Range Explored in This Study	Physical Interpretation
σ^2	~ 0.1–50 [26,27,32,37,41,71]	0.01–100	Enzymatic turnover relative to diffusion within the enzyme layer
β	~ 0.1–25 [9,41,43,71]	0.1–20	External mass transport strength relative to internal diffusion
θ	~ 0.1–10 [9,26,32,41,47,61]	0.1–10	Partition coefficient between enzyme membrane and bulk phases
κ	~ 0.1–10 [2,4,11,26,39]	0.1–10	Relative enzyme affinities

Notes: The definitions of all dimensionless parameters are provided in Table A1. The estimated ranges were obtained by substituting enzyme kinetics values, diffusion coefficients, and membrane thickness values reported in the literature into the corresponding dimensionless definitions. Parameter ranges extending beyond typical estimates were explored parametrically to assess model robustness.

References

1. Turner, A.P.F.; Karube, I.; Wilson, G.S. (Eds.) *Biosensors: Fundamentals and Applications*; Oxford University Press: Oxford, UK, 1990.
2. Scheller, F.W.; Schubert, F. *Biosensors*; Elsevier Science: Amsterdam, The Netherlands, 1992.
3. Malhotra, B.D.; Pandey, C.M. *Biosensors: Fundamentals and Applications*; Smithers Rapra: Shawbury, UK, 2017.
4. Bisswanger, H. *Enzyme Kinetics: Principles and Methods*, 2nd ed.; Wiley-Blackwell: Weinheim, Germany, 2008.
5. Patra, S.; Kundu, D.; Gogoi, M. (Eds.) *Enzyme-Based Biosensors: Recent Advances and Applications in Healthcare*; Springer: Singapore, 2023.

6. López, J.G.; Muñoz, M.; Arias, V.; García, V.; Calvo, P.C.; Ondo-Méndez, A.O.; Rodríguez-Burbano, D.C.; Fonthal, F. Electrochemical and optical carbon dots and glassy carbon biosensors: A review on their development and applications in early cancer detection. *Micromachines* **2025**, *16*, 139. [CrossRef]
7. Sadana, A.; Sadana, N. *Handbook of Biosensors and Biosensor Kinetics*; Elsevier: Amsterdam, The Netherlands, 2011.
8. Cornish-Bowden, A. *Fundamentals of Enzyme Kinetics*, 3rd ed.; Portland Press: London, UK, 2004.
9. Banica, F.G. *Chemical Sensors and Biosensors: Fundamentals and Applications*; John Wiley & Sons: Chichester, UK, 2012; p. 576.
10. Zhou, H.; Guo, W.; Wang, S.; Hao, T.; Wang, Z.; Hu, Y.; Wang, S.; Xie, J.; Jiang, X.; Guo, Z. Electrochemical aptasensor for *Staphylococcus aureus* by stepwise signal amplification. *Microchim. Acta* **2022**, *189*, 353. [CrossRef] [PubMed]
11. Bartlett, P.N. *Bioelectrochemistry: Fundamentals, Experimental Techniques and Applications*; John Wiley & Sons: Chichester, UK, 2008.
12. Lisdat, F. PQQ-GDH—Structure, function and application in bioelectrochemistry. *Bioelectrochemistry* **2020**, *134*, 107496. [CrossRef] [PubMed]
13. Lakard, B. Electrochemical biosensors based on conducting polymers: A review. *Appl. Sci.* **2020**, *10*, 6614. [CrossRef]
14. Izadi, M.; Srivastava, H.M. The reaction-diffusion models in biomedicine: Highly accurate calculations via a hybrid matrix collocation algorithm. *Appl. Sci.* **2023**, *13*, 11672. [CrossRef]
15. Blaedel, W.; Boguslaski, R. Chemical amplification in analysis: A review. *Anal. Chem.* **1978**, *50*, 1026–1032. [CrossRef]
16. Grieshaber, D.; MacKenzie, R.; Vörös, J.; Reimhult, E. Electrochemical biosensors—Sensor principles and architectures. *Sensors* **2008**, *8*, 1400–1458. [CrossRef]
17. Devaux, R.; Bergel, A.; Comtat, M. Mass transfer with chemical reaction in thin-layer electrochemical reactors. *AICHE J.* **1995**, *41*, 1944–1954. [CrossRef]
18. Kulys, J. The development of new analytical systems based on biocatalysts. *Anal. Lett.* **1981**, *14*, 377–397. [CrossRef]
19. Kulys, J.; Vidziunaite, R. Amperometric enzyme electrodes with chemically amplified response. In *Bioinstrumentation*; Wise, D., Ed.; Butterworths: Boston, MA, USA, 1990; pp. 1263–1283.
20. Schubert, F.; Kirstein, D.; Schröder, K.; Scheller, F. Enzyme electrodes with substrate and co-enzyme amplification. *Anal. Chim. Acta* **1985**, *169*, 391–396. [CrossRef]
21. Popovtzer, R.; Natan, A.; Shacham-Diamand, Y. Mathematical model of whole cell based bio-chip: An electrochemical biosensor for water toxicity detection. *J. Electroanal. Chem.* **2007**, *602*, 17–23. [CrossRef]
22. Kulys, J.; Tetianec, L. Highly sensitive biosensor for the hydrogen peroxide determination by enzymatic triggering and amplification. *Sens. Actuator B Chem.* **2006**, *113*, 755–759. [CrossRef]
23. Zhou, C.; Li, X.; Tang, S.W.; Liu, C.; Lam, M.H.W.; Lam, Y.W. A dual-enzyme amplification loop for the sensitive biosensing of endopeptidases. *ACS Omega* **2023**, *8*, 25592–25600. [CrossRef] [PubMed]
24. Ciana, L.D.; Bernacca, G.; Bordin, F.; Fenu, S.; Garetto, F. Highly sensitive amperometric measurement of alkaline phosphatase activity with glucose oxidase amplification. *J. Electroanal. Chem.* **1995**, *382*, 129–135. [CrossRef]
25. Nistor, C.; Rose, A.; Wollenberger, U.; Pfeiffer, D.; Emnéus, J.A. A glucose dehydrogenase biosensor as an additional signal amplification step in an enzyme-flow immunoassay. *Analyst* **2002**, *127*, 1076–1081. [CrossRef]
26. Coche-Guérente, L.; Labbé, P.; Mengeaud, V. Amplification of amperometric biosensor responses by electrochemical substrate recycling. 3. Theoretical and experimental study of the phenol-polyphenol oxidase system immobilized in laponite hydrogels and layer-by-layer self-assembled structures. *Anal. Chem.* **2001**, *73*, 3206–3218. [CrossRef]
27. Baronas, R.; Ivanauskas, F.; Kulys, J. Mathematical model of the biosensors acting in a trigger mode. *Sensors* **2004**, *4*, 20–36. [CrossRef]
28. Croce, R.A.J.; Vaddiraju, S.; Papadimitrakopoulos, F.; Jain, F.C. Theoretical analysis of the performance of glucose sensors with layer-by-layer assembled outer membranes. *Sensors* **2012**, *12*, 13402–13416. [CrossRef]
29. Dagan, O.; Bercovici, M. Simulation tool coupling nonlinear electrophoresis and reaction kinetics for design and optimization of biosensors. *Anal. Chem.* **2014**, *86*, 7835. [CrossRef]
30. Baronas, R.; Žilinskas, A.; Litvinas, L. Optimal design of amperometric biosensors applying multi-objective optimization and decision visualization. *Electrochim. Acta* **2016**, *211*, 586–594. [CrossRef]
31. Varasteanu, P.; Kusko, M. Multi-objective optimization of 2D materials modified surface plasmon resonance (SPR) based sensors: An NSGA II approach. *Appl. Sci.* **2021**, *11*, 4353. [CrossRef]
32. Coche-Guérente, L.; Desprez, V.; Diard, J.P.; Labbé, P. Amplification of amperometric biosensor responses by electrochemical substrate recycling Part I. Theoretical treatment of the catechol-polyphenol oxidase system. *J. Electroanal. Chem.* **1999**, *470*, 53–60. [CrossRef]
33. Schulmeister, T.; Rose, J.; Scheller, F. Mathematical modelling of exponential amplification in membrane-based enzyme sensors. *Biosens. Bioelectron.* **1997**, *12*, 1021–1030. [CrossRef]
34. Sorochinskii, V.; Kurganov, B. Theoretical principles of the application of potentiometric enzyme electrodes. *Appl. Biochem. Microbiol.* **1997**, *33*, 116–124.

35. Sylvia, S.V.; Salomi, R.J.; Rajendran, L.; Lyons, M. Amperometric biosensors and coupled enzyme nonlinear reactions processes: A complete theoretical and numerical approach. *Electrochim. Acta* **2022**, *415*, 140236. [CrossRef]
36. Klos-Witkowska, V.M.A.; Karpinskyi, V. Analysis of stability in enzyme biosensor based on Michaelis-Menten model with time delays. *Acta Phys. Pol. A* **2019**, *135*, 375–379. [CrossRef]
37. Salomi, R.J.; Sylvia, S.V.; Rajendran, L.; Lyons, M. Transient current, sensitivity and resistance of biosensors acting in a trigger mode: Theoretical study. *J. Electroanal. Chem.* **2021**, *895*, 115421. [CrossRef]
38. Elakkya, M.; Swaminathan, R. Mathematical modelling of the phenol-polyphenol oxidase system for amperometric immobilized enzymes at spherical electrode. *Partial. Differ. Equ. Appl. Math.* **2025**, *14*, 101140. [CrossRef]
39. McDonald, A.G.; Tipt, K.F. Parameter reliability and understanding enzyme function. *Molecules* **2022**, *27*, 263. [CrossRef]
40. Britz, D.; Strutwolf, J. *Digital Simulation in Electrochemistry*, 4th ed.; Monographs in Electrochemistry; Springer: Cham, Switzerland, 2016.
41. Lyons, M.E.G. Transport and kinetics at carbon nanotube-redox enzyme composite modified electrode biosensors. *Int. J. Electrochem. Sci.* **2009**, *4*, 77–103. [CrossRef]
42. Schulmeister, T. Mathematical modelling of the dynamic behaviour of amperometric enzyme electrodes. *Sel. Electrode Rev.* **1990**, *12*, 203–260.
43. Baronas, R.; Ivanauskas, F.; Kulys, J. *Mathematical Modeling of Biosensors*, 2nd ed.; Springer Series on Chemical Sensors and Biosensors; Springer: Cham, Switzerland, 2021; Volume 9.
44. Wang, Y.; Pao, C. Time-delayed finite difference reaction-diffusion systems with nonquasimonotone functions. *Numer. Math.* **2006**, *103*, 485–513. [CrossRef]
45. Baronas, R.; Ivanauskas, F.; Kulys, J. The effect of diffusion limitations on the response of amperometric biosensors with substrate cyclic conversion. *J. Math. Chem.* **2004**, *35*, 199–213. [CrossRef]
46. Al-Shannag, M.; Al-Qodah, Z.; Herrero, J.; Humphrey, J.A.; Giralt, F. Using a wall-driven flow to reduce the external mass-transfer resistance of a bio-reaction system. *Biochem. Eng. J.* **2008**, *38*, 554–565. [CrossRef]
47. Benavidez, T.E.; Baruzzi, A.M. Comparative behavior of glucose oxidase and oxalate oxidase immobilized in mucin/chitosan hydrogels for biosensors applications. *Polymer* **2012**, *53*, 438–444. [CrossRef]
48. Skrzypacz, P.; Kabduali, B.; Golman, B.; Andreev, V. Dead-core solutions and critical Thiele modulus for slabs with a distributed catalyst and external mass transfer. *React. Chem. Eng.* **2023**, *8*, 758–762. [CrossRef]
49. Baronas, R. Nonlinear effects of diffusion limitations on the response and sensitivity of amperometric biosensors. *Electrochim. Acta* **2017**, *240*, 399–407. [CrossRef]
50. Dannaoui, R.; Yang, X.K.; Huang, W.H.; Svir, I.; Amatore, C.; Oleinick, A. Importance of diffusional constraints for the quantitative evaluation of calibration curves of enzymatic micro- and nanoelectrochemical sensors. *Electrochim. Acta* **2024**, *473*, 143425. [CrossRef]
51. Baronas, R. Non-monotonic effect of substrate inhibition in conjunction with diffusion limitation on the response of amperometric biosensors. *Biosensors* **2025**, *15*, 441. [CrossRef]
52. Hickson, R.I.; Barry, S.I.; Mercer, G.N.; Sidhu, H.S. Finite difference schemes for multilayer diffusion. *Math. Comput. Model.* **2011**, *54*, 210–220. [CrossRef]
53. Ašeris, V.; Baronas, R.; Petrauskas, K. Computational modelling of three-layered biosensor based on chemically modified electrode. *Comp. Appl. Math.* **2016**, *35*, 405–421. [CrossRef]
54. Baronas, R. Nonlinear effects of partitioning and diffusion-limiting phenomena on the response and sensitivity of three-layer amperometric biosensors. *Electrochim. Acta* **2024**, *478*, 143830. [CrossRef]
55. Blaedel, W.; Kissel, T.; Boguslaski, R. Kinetic behavior of enzymes immobilized in artificial membranes. *Anal. Chem.* **1972**, *44*, 2030–2037. [CrossRef] [PubMed]
56. Jochum, P.; Kowalski, B.R. A coupled two-compartment model for immobilized enzyme electrodes. *Anal. Chim. Acta* **1982**, *144*, 25–38. [CrossRef]
57. Do, T.Q.N.; Varnićic, M.; Hanke-Rauschenbach, R.; Vidakovic-Koch, T.; Sundmacher, K. Mathematical modeling of a porous enzymatic electrode with direct electron transfer mechanism. *Electrochim. Acta* **2014**, *137*, 616–629. [CrossRef]
58. Rafat, N.; Satoh, P.; Worden, R.M. Electrochemical biosensor for markers of neurological esterase inhibition. *Biosensors* **2021**, *11*, 459. [CrossRef]
59. Suganya, S.T.; Rajendran, L.; Lyons, M. Analytical expression of concentrations and current in enzyme-based two-compartment model of amperometric biosensors for steady-state condition. *Int. J. Electrochem. Sci.* **2022**, *17*, 220238. [CrossRef]
60. Velkovsky, M.; Snider, R.; Cliffel, D.E.; Wikswo, J.P. Modeling the measurements of cellular fluxes in microbioreactor devices using thin enzyme electrodes. *J. Math. Chem.* **2011**, *49*, 251–275. [CrossRef]
61. Cussler, E.L. *Diffusion: Mass Transfer in Fluid Systems*, 3rd ed.; Cambridge Series in Chemical Engineering; Cambridge University Press: Cambridge, UK, 2009.

62. Lauverjat, C.; de Loubens, C.; Déléris, I.; Tréléa, I.C.; Souchon, I. Rapid determination of partition and diffusion properties for salt and aroma compounds in complex food matrices. *J. Food Eng.* **2009**, *93*, 407–415. [CrossRef]
63. March, N.G.; Carr, E.J. Finite volume schemes for multilayer diffusion. *J. Comput. Appl. Math.* **2019**, *345*, 206–223. [CrossRef]
64. Samarskii, A. *The Theory of Difference Schemes*; Marcel Dekker: New York, NY, USA, 2001.
65. Britz, D.; Baronas, R.; Gaidamauskaitė, E.; Ivanauskas, F. Further comparisons of finite difference schemes for computational modelling of biosensors. *Nonlinear Anal. Model. Control* **2009**, *14*, 419–433. [CrossRef]
66. Gutfreund, H. *Kinetics for the Life Sciences*; Cambridge University Press: Cambridge, UK, 1995.
67. Wu, M.; Li, L.; Yu, R.; Zhang, Z.; Zhu, B.; Lin, J.; Zhou, L.; Su, B. Tailored diffusion limiting membrane for microneedle glucose sensors with wide linear range. *Talanta* **2024**, *273*, 125933. [CrossRef] [PubMed]
68. Romero, M.R.; Baruzzi, A.M.; Garay, F. Mathematical modeling and experimental results of a sandwich-type amperometric biosensor. *Sens. Actuator B Chem.* **2012**, *162*, 284–291. [CrossRef]
69. Jobst, G.; Moser, I.; Urban, G. Numerical simulation of multi-layered enzymatic sensors. *Biosens. Bioelectron.* **1996**, *11*, 111–117. [CrossRef]
70. Thévenot, D.R.; Toth, K.; Durst, R.A.; Wilson, G.S. Electrochemical biosensors: Recommended definitions and classification. *Biosens. Bioelectron.* **2001**, *16*, 121–131. [CrossRef]
71. Lyons, M.; Bannon, T.; Hinds, G.; Rebouillat, S. Reaction/diffusion with Michaelis-Menten kinetics in electroactive polymer films. Part 2. The transient amperometric response. *Analyst* **1998**, *123*, 1947–1959. [CrossRef]
72. Fink, D.; Na, T.; Schultz, J.S. Effectiveness factor calculations for immobilized enzyme catalysts. *Biotechnol. Bioeng.* **1973**, *15*, 879–888. [CrossRef]
73. Baronas, R. Nonlinear effects of partitioning and diffusion limitation on the efficiency of three-layer enzyme bioreactors and potentiometric biosensors. *J. Electroanal. Chem.* **2024**, *974*, 118698. [CrossRef]
74. Bieniasz, L.; Britz, D. Recent developments in digital simulation of electroanalytical experiments. *Pol. J. Chem.* **2004**, *78*, 1195–1219.
75. Moreira, J.E.; Midkiff, S.P.; Gupta, M.; Artigas, P.V.; Snir, M.; Lawrence, R.D. Java programming for high-performance numerical computing. *IBM Syst. J.* **2000**, *39*, 21–56. [CrossRef]
76. Moberly, J.; Bernards, M.; Waynant, K. Key features and updates for Origin 2018. *J. Cheminform.* **2018**, *10*, 5. [CrossRef]
77. Kulys, J.; Vidziunaite, R. Amperometric biosensors based on recombinant laccases for phenols determination. *Biosens. Bioelectron.* **2003**, *18*, 319–325. [CrossRef]

Disclaimer/Publisher's Note: The statements, opinions and data contained in all publications are solely those of the individual author(s) and contributor(s) and not of MDPI and/or the editor(s). MDPI and/or the editor(s) disclaim responsibility for any injury to people or property resulting from any ideas, methods, instructions or products referred to in the content.